Article

Cell Reports

The Human Cytomegalovirus pUL145 Isoforms Act as Viral DDB1-Cullin-Associated Factors to Instruct Host Protein Degradation to Impede Innate Immunity

Graphical Abstract

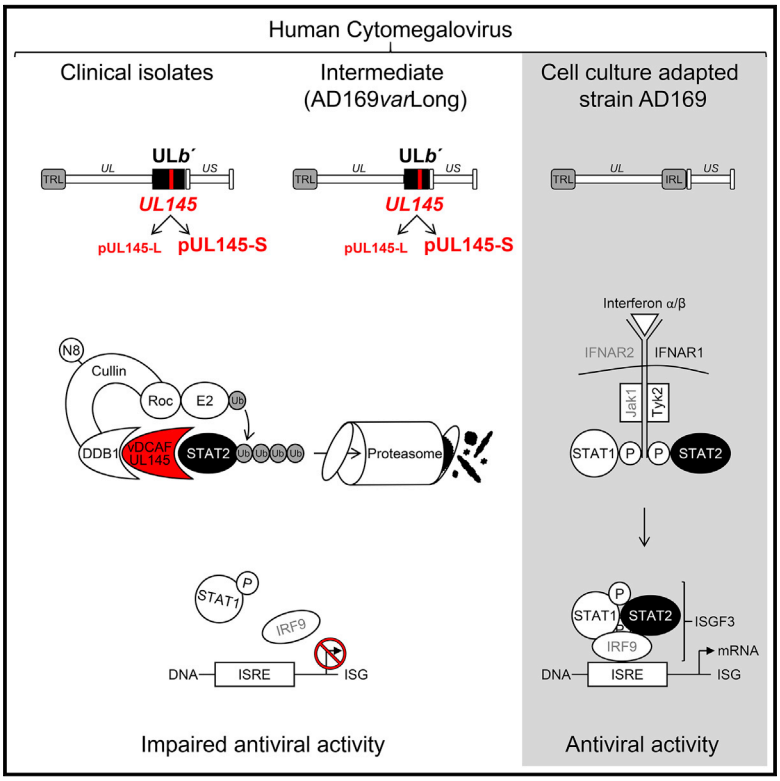

Highlights

- HCMV strains differ in the ULb′ genome region and the capacity to degrade STAT2
- The ULb′ gene *UL145* is associated with a posttranscriptional loss of STAT2
- pUL145s mimic cellular DCAFs and exploit DDB1-cullin RING ubiquitin ligases (CRLs)
- Inhibition of CRLs elicits antiviral activity, which is potentiated by interferon

Authors

Vu Thuy Khanh Le-Trilling, Tanja Becker, Aharon Nachshon, ..., Sebastian Voigt, Hartmut Hengel, Mirko Trilling

Correspondence

khanh.le@uk-essen.de (V.T.K.L.-T.), mirko.trilling@uk-essen.de (M.T.)

In Brief

Le-Trilling et al. utilize intra-strain differences occurring in the HCMV strain AD169 to probe into viral IFN antagonism. They uncover *UL145* as a key factor for HCMV-encoded STAT2 degradation. The pUL145 proteins constitute druggable viral DCAFs (vDCAFs) that mimic the DDB1-recognizing interface of cellular DCAFs to impede antiviral immunity.

Le-Trilling et al., 2020, Cell Reports *30*, 2248–2260
February 18, 2020
https://doi.org/10.1016/j.celrep.2020.01.070

CellPress

OPEN ACCESS
CellPress

Cell Reports
Article

The Human Cytomegalovirus pUL145 Isoforms Act as Viral DDB1-Cullin-Associated Factors to Instruct Host Protein Degradation to Impede Innate Immunity

Vu Thuy Khanh Le-Trilling,[1,6,*] Tanja Becker,[1,6] Aharon Nachshon,[2] Noam Stern-Ginossar,[2] Lara Schöler,[1] Sebastian Voigt,[3,4] Hartmut Hengel,[5] and Mirko Trilling[1,7,*]

[1]Institute for Virology, University Hospital Essen, University of Duisburg-Essen, Essen, Germany
[2]The Department of Molecular Genetics, Weizmann Institute of Science, Rehovot, Israel
[3]Department of Infectious Diseases, Robert Koch Institute, Berlin, Germany
[4]Department of Pediatric Oncology/Hematology/SCT, Charité-Universitätsmedizin Berlin, Berlin, Germany
[5]Institute of Virology, Medical Center and Faculty of Medicine, University of Freiburg, Freiburg, Germany
[6]These authors contributed equally
[7]Lead Contact
*Correspondence: khanh.le@uk-essen.de (V.T.K.L.-T.), mirko.trilling@uk-essen.de (M.T.)
https://doi.org/10.1016/j.celrep.2020.01.070

SUMMARY

Human cytomegalovirus (HCMV) causes diseases in individuals with immature or compromised immunity. To evade immune control, HCMV evolved numerous antagonists targeting the interferon system at multiple levels. By comparative analysis of naturally arising variants of the most widely studied HCMV strain, AD169, and a panel of targeted mutants, we uncover the *UL145* gene as indispensable for STAT2 downregulation. Ribosome profiling confirms the translation of the canonical pUL145 protein (pUL145-Long) and newly identifies a shorter isoform (pUL145-Short). Both isoforms recruit DDB1-containing ubiquitin ligases to induce proteasomal degradation of STAT2. An alanine-scanning mutagenesis discloses the DDB1 interaction motif of pUL145 that resembles the DDB1-binding interface of cellular substrate receptors of DDB1-containing ubiquitin ligases. Thus, pUL145 constitutes a viral DDB1-cullin-associated factor (vDCAF), which mimics cellular DCAFs to exploit the ubiquitin-proteasome system to impede antiviral immunity. Notably, the viral exploitation of the cullins can be targeted to restore the efficacy of the host immune response.

INTRODUCTION

Cytomegaloviruses (CMVs) are prototypical members of β-*herpesvirinae*. The majority of the global adult population is latently infected with human CMV (HCMV). Although fatal infections sporadically occur in apparently healthy individuals (Rafailidis et al., 2008), most HCMV infections in immunocompetent adults progress subclinically. This drastically changes upon conditions of immune immaturity or immunosuppression, during which the control of HCMV is compromised. In the absence of adequate immunity, primary as well as recurrent HCMV infections can cause morbidity and mortality. About 1 in 150 newborns is born with a congenital CMV infection (e.g., https://www.cdc.gov/cmv/congenital-infection.html), leading to thousands of new cases per year in which children have permanent sequelae, such as deafness or intellectual disability (Ludwig and Hengel, 2009). Despite the common practice of CMV diagnostics of transplant patients as well as universal prophylaxis or preemptive therapy, the CMV serostatus of donor and recipient significantly affects the overall survival of transplant recipients (Ljungman et al., 2014; Schmidt-Hieber et al., 2013). Another cohort of people with CMV disease (e.g., retinitis and blindness) is people living with AIDS (e.g., Heiden et al., 2014). Although several antiviral drugs are approved to treat CMV disease, their application is limited by side effects, teratogenicity, embryotoxicity, and the occurrence of antiviral drug resistance. Thus, the identification of new drug targets is of particular clinical relevance.

Productive phases of CMV replication are normally controlled by a concerted effort of all branches of the immune system. Nevertheless, clearance is never achieved since latent CMV genomes remain. To enable efficient viral replication despite the presence of host immune responses, CMVs evolved a remarkable array of antagonists targeting intrinsic, innate, and adaptive immunity (Hengel et al., 1998; Le-Trilling and Trilling, 2015; Loenen et al., 2001; Powers et al., 2008). One important pillar of the immune system is the interferon (IFN) response. Upon pathogen encounter, cells secrete IFNs to establish an antiviral state, to reinforce intrinsic immunity, and to stimulate and orchestrate adaptive immunity (Samuel, 2001; Sen, 2001; Stark et al., 1998). By binding to their cognate receptors, IFNs signal via receptor-associated Janus kinases (JAK) to activate signal transducer and activator of transcription (STAT) proteins by phosphorylation (Stark and Darnell, 2012). Activated STAT dimers translocate to the nucleus to regulate the expression of cellular IFN-stimulated genes (ISGs) and IFN-repressed genes (IRepGs) (Megger et al., 2017; Trilling et al., 2013). In the absence of STAT1 or STAT2, the host succumbs a few days after CMV infection, as shown by studies using mouse CMV (MCMV)

(Gil et al., 2001; Le-Trilling et al., 2018). Given the selection pressure elicited by the IFN system, it is not surprising that HCMV interferes with several steps of the IFN signaling cascade, such as the downregulation of JAK1, JAK2, IRF9, and STAT2 (Le Roy et al., 1999; Le et al., 2008; Miller et al., 1998, 1999; Weekes et al., 2014). However, the responsible viral gene products mediating these inhibitory effects are still elusive. The ability to degrade STAT2 was observed for clinical HCMV strains and for some laboratory strains (Le et al., 2008). Since increasing data become available that describe genomic alterations assembled during HCMV cell culture passaging (e.g., Cha et al., 1996; Dargan et al., 2010; Murphy et al., 2003), we reasoned that differences among HCMV strains and variants may be instrumental in identifying viral gene products responsible for phenotypes such as the impaired IFN antagonism. The HCMV double-strand DNA (dsDNA) genome is composed of two unique regions, the unique long (UL) and unique short (US) regions, which are flanked by inverted repeats. According to their association, the repeats of the UL and US regions are named repeat long (RL) and repeat short (RS), respectively. AD169 was the first HCMV strain that was sequenced and annotated (Chee et al., 1990) and that was, and still is, used for numerous studies. The AD169 genome is considered to differ from clinical isolates by its lack of the so-called ULb′ region, which is located at the boundary of the UL and b′ RL regions. However, HCMV AD169 variants were identified that retained large parts of the ULb′ region (Bradley et al., 2009; Le et al., 2011). AD169 variants with long (AD169variantLong) and short (AD169variantShort) UL genome regions differ concerning 11.8 kb of coding capacity comprising ULb′ genes.

The apparently strain-dependent ability of HCMV to downregulate STAT2 (Le et al., 2008) prompted us to compare the AD169 variants concerning their antagonistic effects on the IFN signaling cascade. We discovered that the ULb′ gene *UL145* is essential for inducing the degradation of STAT2. Remarkably, ribosome profiling data disclosed the existence of two pUL145 isoforms, the canonical protein and a newly identified shorter isoform, which we termed pUL145-Long and pUL145-Short, respectively. pUL145-Short is expressed earlier and more abundantly, thus constituting the main gene product of *UL145* in infected fibroblasts. Both pUL145 isoforms recruit cellular DDB1-containing ubiquitin ligase complexes via a motif that exhibits similarities to the binding interface of cellular substrate receptors of the DDB1/ubiquitin ligase complexes, the DDB1-cullin-associated factors (DCAFs). Our mechanistic analyses of viral immune evasins exploiting the ubiquitin-proteasome system extend the molecular in-depth understanding and may be instrumental to identifying novel drug targets and treatments that rely on the druggability of cullin RING ubiquitin ligases (CRLs).

RESULTS

HCMV ULb′ Gene Products Contribute to the Inhibition of the IFN Signaling and Influence IFN Susceptibility

The STAT2 antagonistic capacities differ among HCMV strains (Le et al., 2008), and HCMV strains differ regarding the presence or absence of the ULb′ region. Thus, we hypothesized that the STAT2 degradation may be executed by a protein encoded or regulated by a ULb′ gene product. Consistent with this idea, clinical HCMV isolates, AD169variantLong, and a previously described (Le et al., 2011) bacterial artificial chromosome (BAC)-based clone of the AD169variantLong reduce STAT2 levels during infection (Figure S1A).

BAC technology yields clonal viral genomes. The analysis of high numbers of BAC clones, which were generated from AD169variantLong-infected cultures, revealed that the parental virus stock represents a mixture of ULb′-positive and ULb′-negative viruses, as a small fraction (<10%) of BAC clones lacked the ULb′ region. In this case, BAC-DNA restriction analyses and sequence determinations showed a genome organization identical to AD169variantShort (Figures S1B and 1A). This finding implies that AD169variantLong is a direct ancestor of the widely used AD169 laboratory strain. Using the two representative BAC-derived clones AD169-BAC2 and AD169-BAC20, which genetically correspond to AD169variantLong and AD169variantShort, respectively, we confirmed similar replication capacities in fibroblast culture (Figure S1C). For convenience, we named the AD169-BAC2- and AD169-BAC20-derived viruses AD169varL and AD169varS, respectively.

We determined the protein levels of STAT2 as well as JAK1, JAK2, and IRF9 in AD169varL- and AD169varS-infected cells. These components of the IFN signaling cascade were shown to be downregulated by HCMV, but the responsible viral gene products are still elusive. We observed that both AD169 variants downregulated JAK1 and IRF9 (Figure 1B). However, the reduction of STAT2 and JAK2 was restricted to cells infected with AD169varL (Figure 1B). Interestingly, HCMV infection induced the occurrence of a smaller protein that was recognized by the JAK2 antibody (Figure 1B). To test the biological relevance of the difference in terms of IFN antagonism, we infected IFNα- and IFNγ-conditioned cells with AD169varL and AD169varS reporter viruses expressing EGFP. Although AD169varS exhibits impaired downregulation of STAT2 and JAK2, the IFN signaling cascade is effectively and redundantly controlled by JAK1 and IRF9 downregulation (Figure 1B). This may explain why AD169varS only showed a minor and borderline-significant ($p = 0.052$) increase in IFNα susceptibility (Figure 1C). Consistent with previous publications (Le et al., 2008; Sainz et al., 2005), IFNγ pre-treatment elicited stronger antiviral activity, compared to IFNα, as evident by reduced EGFP expression (Figure 1C). Additionally, we observed that the lack of the ULb′ region was associated with a significantly reduced ability to replicate in IFNγ-conditioned cells (Figure 1C). When we compared the replication of AD169varL and AD169varS in IFNβ- and IFNγ-treated cells, we observed that AD169varS exhibits a significantly increased susceptibility to type I and type II IFNs (Figure 1D).

Ribosome Profiling of AD169varL and AD169varS Viruses Specifies Distinct Expression of Viral Genes

Our analyses showed that the AD169 variants differ in their capacity to antagonize IFN signaling. Based on ribosome profiling and transcript analyses, we globally defined the genes that are differentially expressed by AD169varL and AD169varS in order to determine the IFN antagonist(s). Complete sequencing of both BAC-cloned genomes, combined with ribosome profiling analysis, enabled us to annotate and compare the

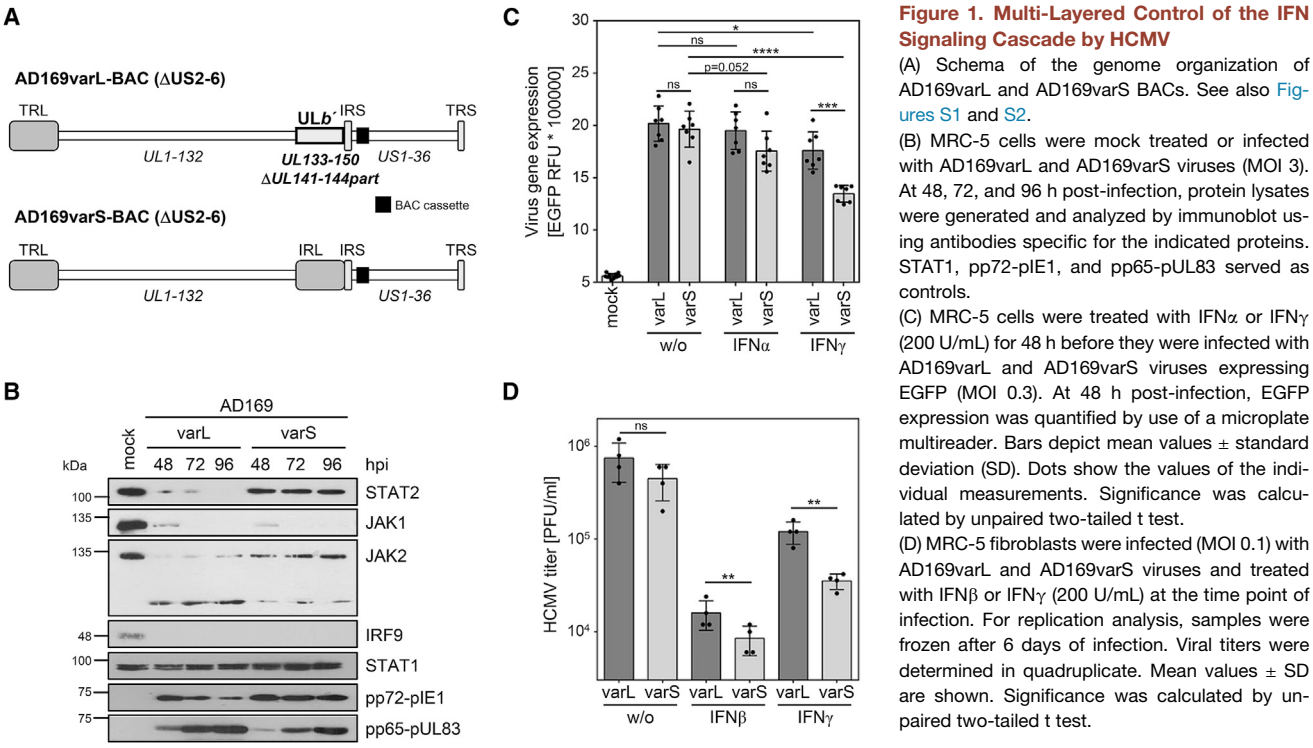

Figure 1. Multi-Layered Control of the IFN Signaling Cascade by HCMV

(A) Schema of the genome organization of AD169varL and AD169varS BACs. See also Figures S1 and S2.

(B) MRC-5 cells were mock treated or infected with AD169varL and AD169varS viruses (MOI 3). At 48, 72, and 96 h post-infection, protein lysates were generated and analyzed by immunoblot using antibodies specific for the indicated proteins. STAT1, pp72-pIE1, and pp65-pUL83 served as controls.

(C) MRC-5 cells were treated with IFNα or IFNγ (200 U/mL) for 48 h before they were infected with AD169varL and AD169varS viruses expressing EGFP (MOI 0.3). At 48 h post-infection, EGFP expression was quantified by use of a microplate multireader. Bars depict mean values ± standard deviation (SD). Dots show the values of the individual measurements. Significance was calculated by unpaired two-tailed t test.

(D) MRC-5 fibroblasts were infected (MOI 0.1) with AD169varL and AD169varS viruses and treated with IFNβ or IFNγ (200 U/mL) at the time point of infection. For replication analysis, samples were frozen after 6 days of infection. Viral titers were determined in quadruplicate. Mean values ± SD are shown. Significance was calculated by unpaired two-tailed t test.

coding capacities and the translatome of both variants. Sequence comparisons revealed a high degree of sequence conservation of AD169 variants from different laboratories since only few SNPs were found (Table S1). Most of the non-ULb′ genes were expressed by both AD169varL and AD169varS to similar levels (Figure 2A; see also Table S2, which lists the normalized number of reads per kilobase per million [RPKM] calculated for coding sequence (CDS) regions of AD169varL and AD169varS). As expected, the duplication of the RL sequence resulted in an increased expression of the respective RL genes (Figures 2B and S1D). This finding was confirmed by an assessment of abundance of the viral Fc-binding protein gp34-pRL11 (Atalay et al., 2002) (Figure S1E). Nevertheless, the most prominent difference between both AD169 variants was the translation of ULb′ genes during AD169varL infection but not during AD169varS infection (Figures 2A and 2B, lower right quadrant).

The ribosome footprints specified the ULb′ gene products expressed by AD169varL. The canonical ULb′ genes *UL148*, *UL147A*, *UL147*, *UL146*, *UL145*, *UL139*, *UL138*, *UL136*, *UL135*, *UL133*, *UL148A/B/C/D*, *UL150A*, and *UL150* were efficiently translated in AD169varL-infected cells. In addition, translation from regions of several recently annotated ULb′ gene products was detected (Figures S2 and 2C; Table S3), affirming the high complexity of HCMV gene expression during productive infection. This analysis also revealed viral genes, which were not detected (below the cutoff of 10 RPKM) in both AD169varL- and AD169varS-infected cells. This group of genes comprises the *US2-6* region, which is replaced by the BAC cassette, 12 non-ULb′ open reading frames (ORFs), and 17 ORFs, which are located in the part of the ULb′ region (*UL140-144*) that is deleted from the AD169varL genome (Table S3). Taken together, our analyses provide an in-depth annotation of the coding capacities of two clonal and genetically modifiable AD169 variants. The data constitute a profound basis for comparative analyses of distinct phenotypes, not only for our study but also for future work.

Identification of the ULb′ Gene Product UL145 as a STAT2 Antagonist

Since our analyses indicated that ULb′ proteins contribute to the multi-layered inhibition of IFN signaling, an approach of systematic mutagenesis was conducted to identify the ULb′-encoded IFN antagonist(s). We constructed a panel of HCMV mutants harboring deletions of 2 to 11.8 kb covering the entire AD169 ULb′ region (see Figure 3A for a schematic overview). Using these mutants, we screened for the gene(s) responsible for STAT2 downregulation (Figure 3B). Interestingly, the viral downmodulation of STAT2 could be prevented by deletion of the ULb′ region, but the loss of JAK2 still occurred in cells infected with the AD169varL mutant lacking all ULb′ genes (Figure 3B; ΔUL148-150). This finding suggests that a non-ULb′ gene product, which is differentially expressed by AD169varL and AD169varS, encodes the JAK2 inhibitor(s).

Our analysis of the AD169varL ULb′ deletion mutants narrowed down the gene region encoding the STAT2 inhibitor to *UL145* to *UL140/144*. However, the AD169varL ULb′ region exhibits an internal deletion spanning the complete sequence of *UL141* and *UL142* as well as parts of *UL140* and *UL144*. The deletion creates an abnormal *UL140/144* fusion ORF consisting

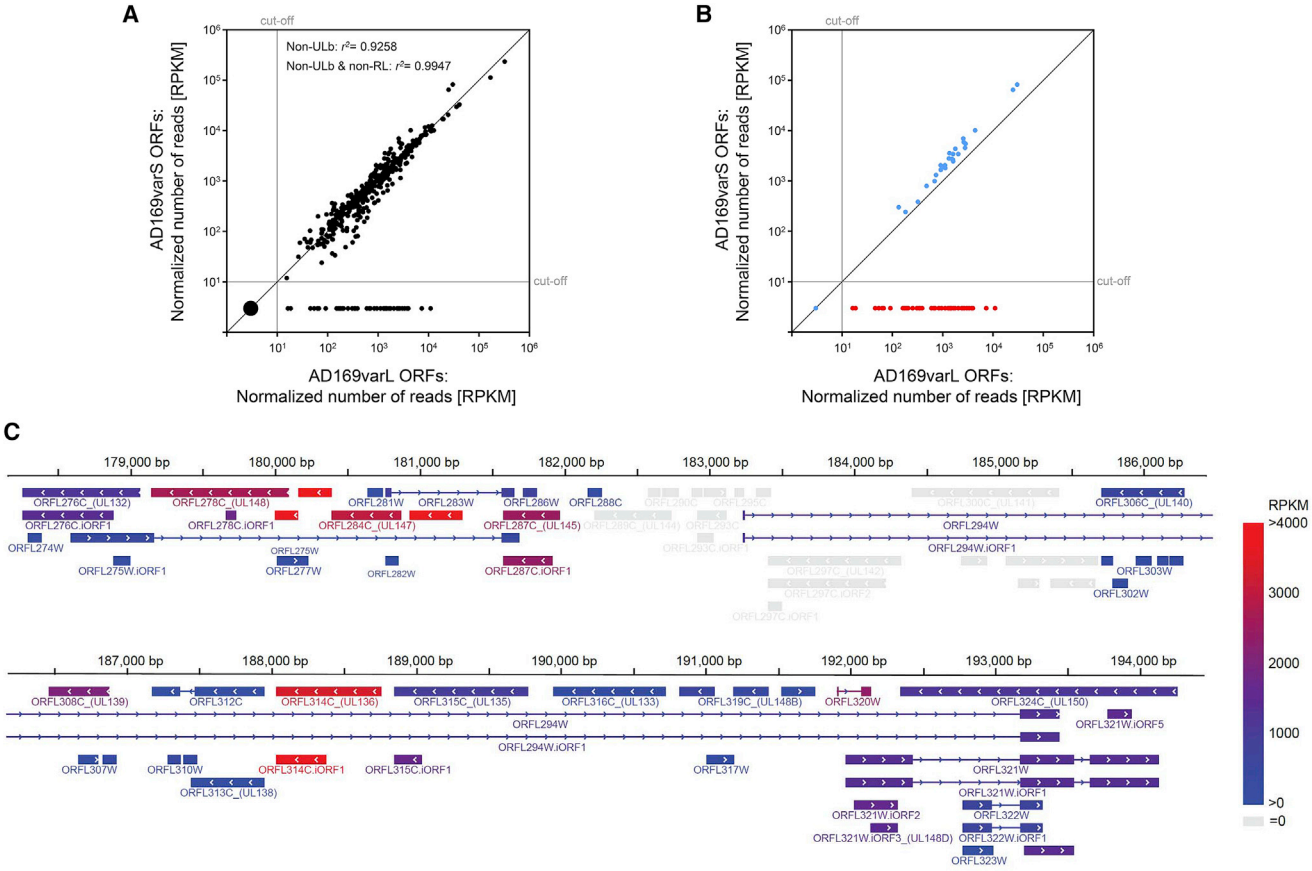

Figure 2. Ribosome Profiling Analyses of AD169varL and AD169varS Viruses Specify Distinct Expression of Viral Genes

(A) MRC-5 cells were infected with AD169varL and AD169varS. At 72 h post-infection, cells were harvested in the presence of cycloheximide, and ribosome footprints were extracted and sequenced. The diagram shows the normalized number of reads (reads per kilobase per million, RPKM) calculated for CDS regions of AD169varS versus those of AD169varL.

(B) To highlight the RL and ULb′ ORFs, these data points were shown without all other ORFs.

(C) The ribosome footprints of the AD169varL ULb′ ORFs were aligned to the Merlin annotation and colored according to the profiling RPKM values to visualize the expression levels. Please note that the AD169varL ULb′ region exhibits an internal deletion resulting in (partial) loss of *UL141* to *UL144*.

See also Figures S1 and S2 and Tables S1, S2, and S3.

of most of the *UL140* sequence fused to a partial *UL144* sequence, making an interaction between UL140/144 and STAT2 unlikely. Thus, we focused on *UL145* and constructed an AD169varL-based ΔUL145 mutant. We tested this mutant virus and observed a STAT2 recovery in ΔUL145-infected cells (Figure 3C). To corroborate this finding, we additionally constructed a TB40-BAC4-based ΔUL145 mutant. We found that the deletion of *UL145* from the TB40 genome also resulted in a recovery of STAT2 (Figure 3D). To ensure that pUL145 is the STAT2 antagonist, we constructed the revertant virus AD169varLΔUL145:UL145-HA by introducing an expression cassette, which comprises the cellular EF1 promoter and the *UL145* coding sequence with a C-terminal hemagglutinin (HA) epitope-tag, into the *UL145* locus. We confirmed the expression of pUL145-HA and verified that the presence of pUL145 reestablished the downregulation of STAT2 (Figure 3E).

Having shown that *UL145* is required for STAT2 reduction, we went on to test if pUL145 depends on viral co-factors. We cloned the *UL145* coding sequence into expression plasmids and tested the IFN-inhibitory capacity in ectopic expression using an interferon-stimulated response element (ISRE)-dependent luciferase reporter to quantify IFN-induced gene expression. The MCMV-encoded STAT2 antagonist pM27 (Le-Trilling et al., 2018; Trilling et al., 2011; Zimmermann et al., 2005) served as a positive control. We found that ectopically expressed pUL145 was sufficient to prevent IFNα-induced gene expression in a dose-dependent manner (Figure 3F). To confirm that the observed pUL145-mediated inhibition of the IFN response is based on STAT2 downregulation, we co-expressed STAT2 with pUL145, pM27, or a control plasmid and detected STAT2 levels. The efficiency of the downregulation of co-expressed STAT2 correlated with the amount of transfected UL145 and M27 plasmids (Figure 3G). Since we have previously shown that HCMV mediates STAT2 reduction post-transcriptionally through proteasomal degradation (Le et al., 2008), we inferred a physical interaction of pUL145 and STAT2. To test this, we conducted co-immunoprecipitation (coIP) experiments. STAT2 degradation was prevented by adding MG132, an inhibitor of

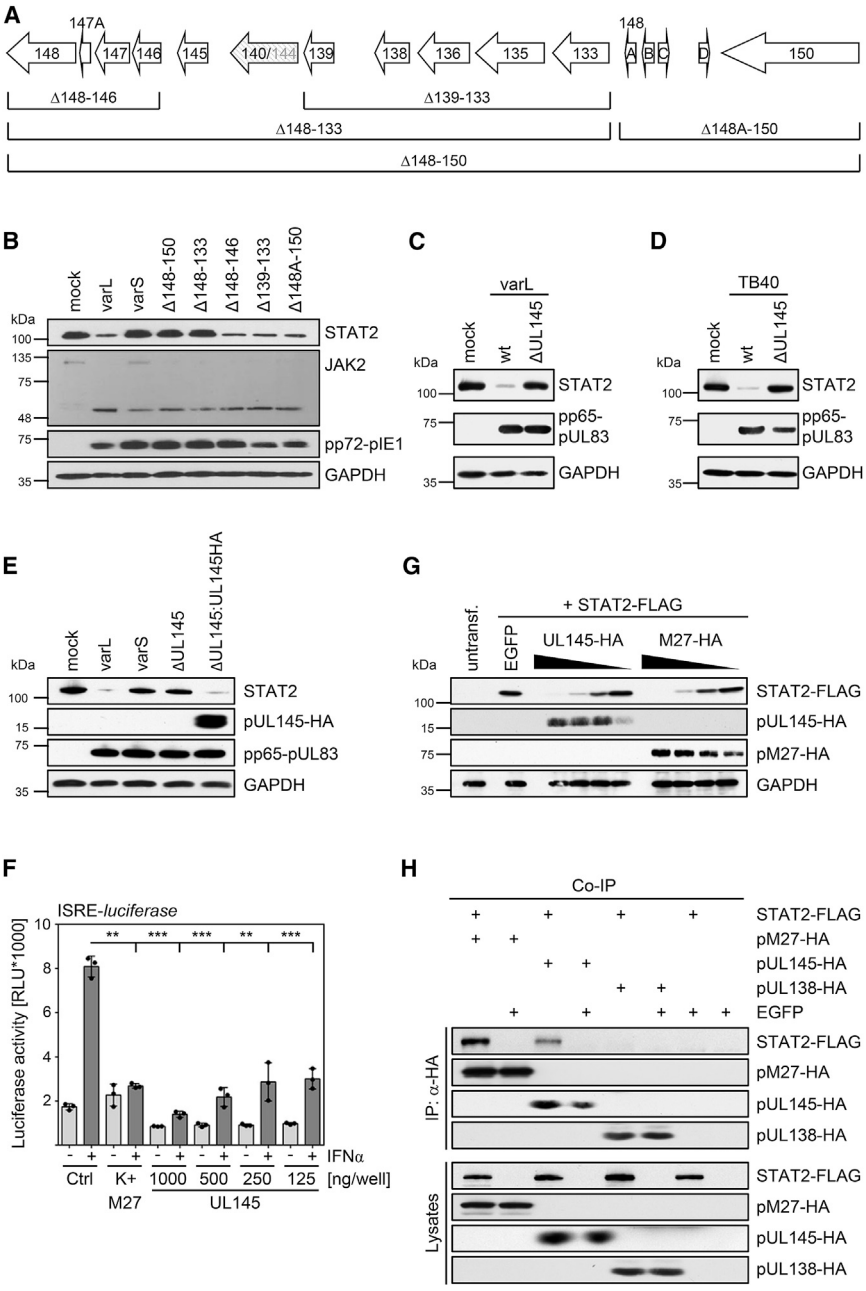

Figure 3. Identification of UL145 as a STAT2 Antagonist

(A) Schema of the canonical AD169 ULb′ ORFs. Please note that the order of the ULb′ genes in the AD169 genome does not match with the UL nomenclature. The ORFs that are deleted in the respective HCMV mutants are schematically depicted.

(B) MRC-5 cells were infected with the indicated viruses (MOI 3). At 72 h post-infection, protein lysates were generated and analyzed by immunoblot using antibodies specific for the indicated proteins.

(C) MRC-5 cells were mock treated or infected with AD169varL and AD169varLΔUL145 (MOI 3). At 96 h post-infection, protein lysates were generated for immunoblot analysis using antibodies specific for the indicated proteins.

(D) MRC-5 cells were mock treated or infected with TB40 and TB40ΔUL145 (MOI 3). At 96 h post-infection, protein lysates were generated for immunoblot analysis.

(E) MRC-5 cells were infected with AD169varL, AD169varS, AD169varLΔUL145, and AD169varLΔUL145:UL145HA (MOI 3). At 72 h post-infection, protein lysates were generated and analyzed by immunoblot.

(F) HeLa cells were co-transfected with pISRE luciferase reporter plasmid and the indicated amounts of M27 or UL145 expression construct. At 16 h post-transfection, the cells were treated with 150 U/mL IFNα for 5 h before they were lysed. Luciferase activity was determined. Each condition was measured in triplicate. Mean values ± SD are shown. Significance was calculated by unpaired two-tailed t test.

(G) HeLa cells were transfected with the indicated combinations of STAT2-FLAG expression construct and pIRES-EGFP:UL145-HA, pIRES-EGFP:M27-HA, or empty pIRES-EGFP vector. UL145-HA and M27-HA plasmids were used in graded concentrations. The overall DNA amount of each transfection sample was normalized by adding the respective amount of empty vector. At 24 h post-transfection, protein lysates were generated and analyzed by immunoblot using antibodies detecting the indicated proteins.

(H) 293T cells were transfected with the indicated plasmids. At 16 h post-transfection, cells were treated with MG132 (10 μM) for 3.5 h before lysates were generated, and an immunoprecipitation (IP) with an HA-specific antibody was performed. The lysates and the IP samples were analyzed by immunoblot to test STAT2 co-precipitation.

See also Figure S3.

the proteasome. The STAT2 interacting protein pM27 and the HCMV protein pUL138 served as positive and negative controls, respectively. Indeed, STAT2 was co-purified when pUL145 was precipitated (Figure 3H), indicating a physical interaction. Accordingly, the direct precipitation of STAT2 retrieved pUL145 (Figure S3A). Our results show that pUL145 binds STAT2 and is sufficient and essential for its degradation.

The *UL145* Locus Codes for Two UL145 Isoforms

Making use of the comprehensive translation data obtained by ribosome profiling, we checked the annotation as well as the ribosome footprints of the *UL145* gene region. This analysis suggested the existence of two UL145 isoforms: ORFL287C_UL145 and ORFL287C.iORF1. Previously published data of Merlin- and TB40-infected fibroblasts (Stern-Ginossar et al., 2012) suggest that both isoforms are efficiently translated during infection (Figure S3B). The *UL145* ribosome footprints of AD169varL-infected cells resemble those of Merlin- and TB40-infected cells (Figure S3B). The canonical pUL145 isoform, ORFL287C_UL145, represents an N-terminal extended form of the isoform ORFL287C.iORF1. Therefore, we termed them UL145-Long (UL145-L) and UL145-Short (UL145-S), respectively (Figure 4A).

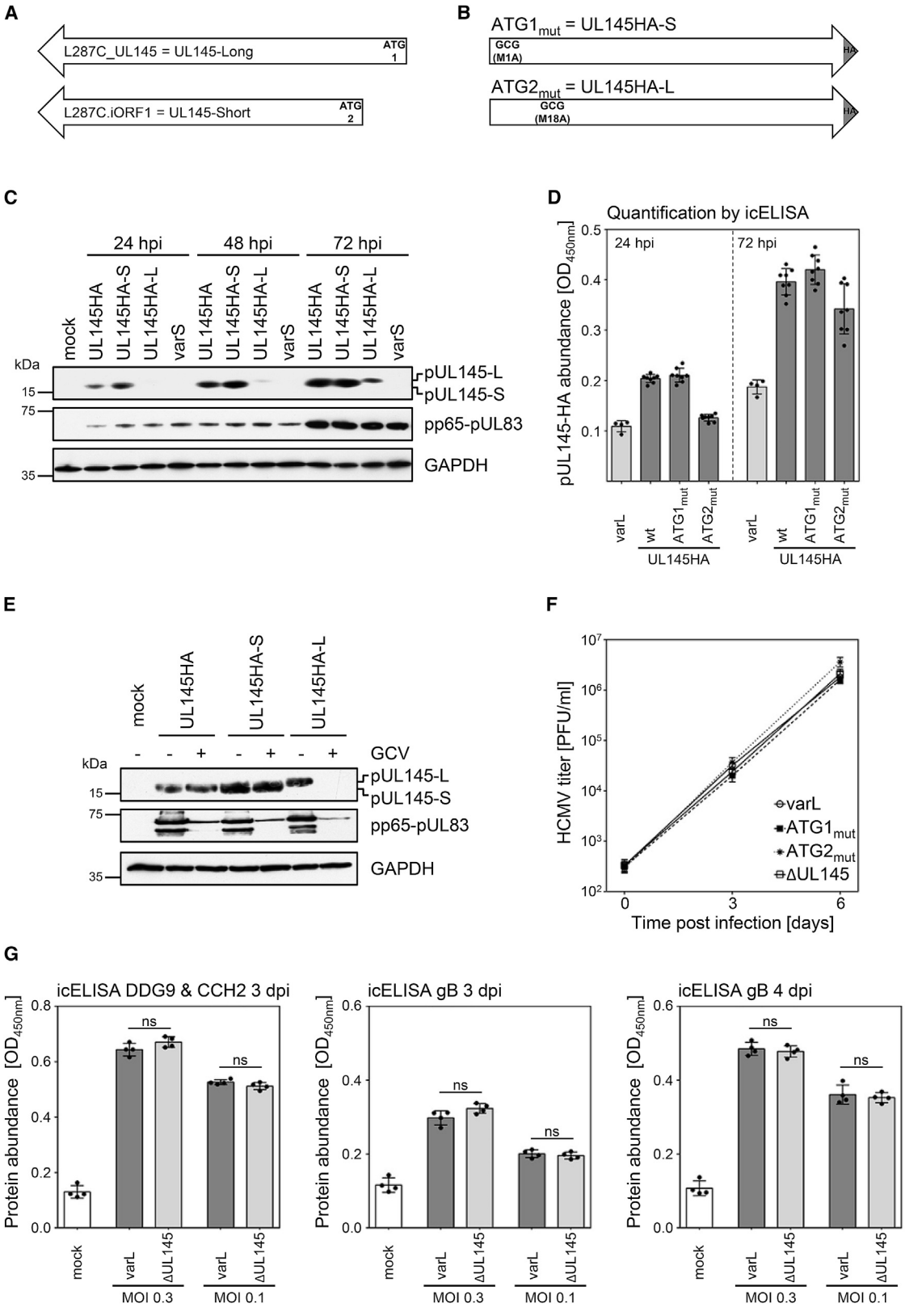

(legend on next page)

Ribosome profiling provides information about the translation, while corresponding proteins are not quantified. Obviously, protein abundances are not only influenced by the rate of synthesis but also by the rate of decay. To test the existence of both pUL145 proteins during infection, we generated an HCMV expressing pUL145 with a C-terminal HA-tag (UL145HA). Subsequently, we mutated the start codons of both UL145 isoforms (Figure 4B), resulting in the viruses UL145HA:ATG1mut and UL145HA:ATG2mut, which express only pUL145HA-Short and pUL145HA-Long, respectively. Using these viruses, we verified the expression of both pUL145 protein isoforms during infection (Figure 4C). We observed that pUL145-S and pUL145-L are expressed with distinct kinetics. Intriguingly, the newly identified pUL145-S protein is expressed earlier and more abundantly—as shown by western blot analysis and quantified by icELISA (Figures 4C and 4D)—thus constituting the major pUL145 protein isoform. Since pUL145-L is detected only later during infection, we applied the drug ganciclovir (GCV) to inhibit viral replication and prevent late gene expression. Interestingly, the levels of pUL145-S were not altered by GCV treatment, whereas the amount of pUL145-L was clearly reduced (Figure 4E). Accordingly, only pUL145-S was detectable in semi-permissive cells, in which viral late gene expression is diminished (data not shown). When we visualized the *UL145* mRNAs by northern blot, we detected a short *UL145* transcript, which was expressed earlier and more abundantly than the longer *UL145* transcript (Figure S3C). The elimination of one or both pUL145 isoforms by mutagenesis did not impair HCMV replication capacity or the abundance of viral proteins like gB (Figures 4F and 4G).

Our results show that the previously known canonical pUL145-L isoform is barely detectable by immunoblot at early times of infection and strongly suggest that most of the observed pUL145 function is actually mediated by the newly identified pUL145-S protein. It will be interesting to test if that also holds true for other functions of pUL145 (e.g., the interference with intrinsic immunity by helicase-like transcription factor [HLTF] degradation) (Nightingale et al., 2018).

pUL145 Recruits DDB1 via a DCAF-like Interaction Motif to Antagonize IFN Signaling by STAT2 Degradation

Our experiments showed similarities between the newly identified HCMV antagonist, pUL145, and the known MCMV-encoded STAT2 inhibitor pM27. Since pM27 recruits DDB1 to exploit cellular CRLs for poly-ubiquitination and proteasomal degradation of STAT2 (Landsberg et al., 2018; Trilling et al., 2011), and proteasomal inhibitors as well as the CRL inhibitory drug MLN4924 restore STAT2 in HCMV-infected cells (Le-Trilling et al., 2016; Le et al., 2008), we tested if pUL145 also exploits DDB1 and associated CRLs for STAT2 degradation. To analyze this in the infection context, we constructed a recombinant HCMV based on the AD169varS background, which expresses an HA-tagged version of pUL145 under the control of the cellular EF1 promoter (AD169varS:UL145-HA). We observed that pUL145 co-precipitated DDB1 in infected cells, even in the absence of other ULb′ proteins (Figure 5A). This finding is consistent with a recent study by Nightingale et al. (2018). To test the functional relevance of the DDB1 interaction, we applied the drug MLN4924, which abrogates CRL activity by blocking the activity-defining Nedd8 conjugation of cullins (Soucy et al., 2009). MLN4924 restored STAT2 levels in AD169varL-infected cells, but not in uninfected cells (Figure 5B), indicating that pUL145 exploits DDB1 and the associated CRLs to induced proteasomal degradation of STAT2. Similarly, HLTF was also restored upon MLN4924 treatment (Figure S3D). Consistent with our previous mass spectrometry (MS) data (Le-Trilling et al., 2016), MLN4924 treatment decreased STAT2 amounts in uninfected cells. This may be explained by an increased abundance of STAT2-destabilizing proteins. Accordingly, CRLs negatively regulate the stability of F-Box protein W7 (FBXW7) (Emanuele et al., 2011), which is known to destabilize STAT2 (Lee et al., 2020). Furthermore, the decreased level of the late gene product pp28-pUL99 reflects the described antiviral activity of MLN4924 (Le-Trilling et al., 2016). Having shown that two pUL145 isoforms are expressed during HCMV infection, we asked if pUL145-S is sufficient to recruit DDB1-containing ubiquitin ligase complexes to mediate STAT2 degradation. Therefore, we used the mutants, which express only pUL145HA-S and pUL145HA-L, and examined co-precipitation of DDB1 and levels of STAT2 late after infection to ensure sufficient pUL145-L abundance. Both pUL145 isoforms recruited DDB1 and downregulated STAT2 (Figures 5C and 5D).

In contrast to other primate CMVs, only human and panine CMV encode pUL145 proteins with an extended N terminus (Figure 6A). The alignment of the amino acid sequences of pUL145-homologous proteins encoded by primate CMVs disclosed a number of highly conserved residues (Figure 6A). The M18A mutation introduced to distinguish between pUL145-L and pUL145-S did not impair the interaction with DDB1 (Figure 6B). We constructed a

Figure 4. The *UL145* Locus Codes for Two UL145 Isoforms

(A) Schema of the two *UL145* isoforms identified by ribosome profiling (Stern-Ginossar et al., 2012). See also Figure S3.

(B) For the analysis of the individual UL145 isoforms, the start codons ATG1 and ATG2 were mutated to express only UL145-Short (UL145-S) and UL145-Long (UL145-L), respectively.

(C) MRC-5 cells were infected with indicated viruses. At 24, 48, and 72 h post-infection, lysates were generated for immunoblot analysis of indicated proteins.

(D) MRC-5 cells were infected with indicated viruses. At 24 and 72 h post-infection, cells were fixed and analyzed by icELISA using an anti-HA antibody to quantify the amount of UL145HA proteins in infected cells. Bars depict mean values ± SD. Dots show the values of the individual measurements.

(E) MRC-5 cells were infected in the absence and presence of the late gene inhibitor ganciclovir (GCV; 50 μM). At 72 h post-infection, lysates were generated for analysis of indicated proteins.

(F) MRC-5 fibroblasts were infected (MOI 0.1) with AD169varL, ATG1mut, ATG2mut, and ΔUL145 viruses. For replication analysis, samples were frozen after 3 and 6 days of infection. Viral titers were determined in quadruplicate. Mean values ± SD are shown.

(G) MRC-5 cells were infected with AD169varL and ΔUL145. At indicated times post-infection, cells were fixed and analyzed by icELISA using the indicated antibody to quantify the amount of viral proteins in infected cells. Bars depict mean values ± SD. Dots show the values of the individual measurements. Significance was calculated by unpaired two-tailed t test.

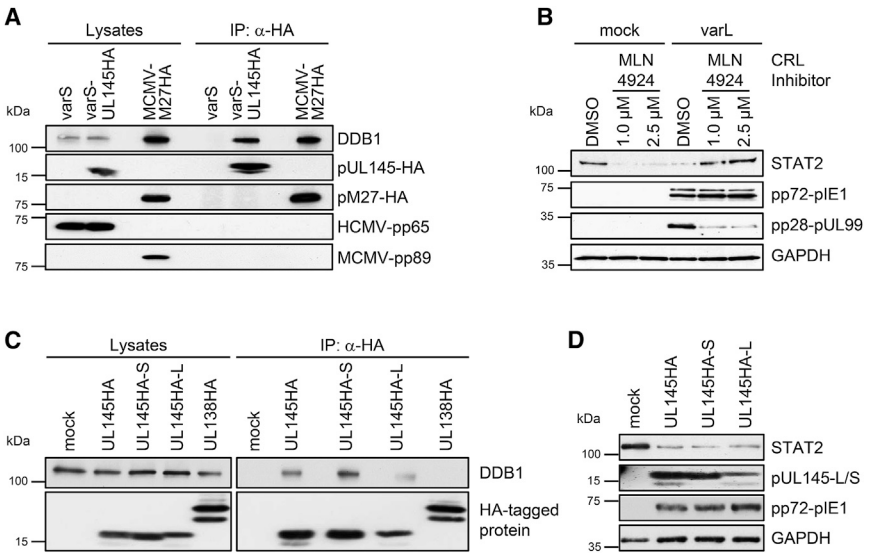

Figure 5. The pUL145 Isoforms Recruit DDB1-Containing CRLs to Induce STAT2 Degradation

(A) MRC-5 cells were infected with AD169varS and AD169varS:UL145HA (MOI 3). At 72 h post-infection, lysates were generated, and an IP with an HA-specific antibody was performed. The lysates and the IP samples were analyzed by immunoblot to test DDB1 co-precipitation. Mouse fibroblasts infected with an MCMV expressing M27-HA were used as a control.

(B) MRC-5 fibroblasts were infected with AD169varL (MOI 5). At 15 h post-infection, cells were treated with MLN4924 (indicated concentration). At 48 h post-infection, lysates were generated for immunoblot analysis of indicated proteins. See also Figure S3.

(C) MRC-5 cells were infected with the indicated viruses. At 72 h post-infection, lysates were generated, and an IP with an HA-specific antibody was performed. The lysates and the IP samples were analyzed by immunoblot to test DDB1 co-precipitation. The UL138HA-expressing virus served as the control for the specificity of the DDB1 interaction.

(D) MRC-5 cells were infected with indicated viruses (MOI 5). At 72 h post-infection, lysates were generated for immunoblot analysis of indicated proteins.

comprehensive panel of pUL145 mutants by replacing the conserved amino acids by alanine and then tested these pUL145 mutants for their ability to co-precipitate DDB1 to identify pUL145 interaction motifs. The analysis of these mutants revealed that conserved residues located at the N terminus of pUL145-L and pUL145-S are crucial for the interaction of pUL145 with DDB1 (Figure 6C). Hence, we examined this motif in more detail. We compared the pUL145 motif with cellular DDB1-interacting proteins and found this motif to resemble the H-box motif (Li et al., 2010) of the DDB1-binding interface of DCAFs (Figure 6D). The DCAF proteins constitute a family of substrate receptors of the DDB1/ubiquitin ligase complexes and thereby determine substrate recognition (Lee and Zhou, 2007). To ensure that the conserved residues of this motif are indeed decisive for the DDB1 interaction, we generated an additional set of pUL145 mutants comprising the entire motif. The analysis of the mutants was fully consistent with the relevance of the DCAF-like motif. In particular, the residues N25, L30, and R33, which are conserved throughout the DCAF motifs, were indispensable for DDB1 binding of pUL145 (Figure 6E). Interestingly, R35, which is highly conserved among primate CMV pUL145 homologs but lacking in the cellular DCAF motif, is also essential for the DDB1 interaction (Figure 6E). This finding indicates that this amino acid is positioned in a key structure of the pUL145 protein, which is pivotal for the recruitment of DDB1. Intrigued by the relevance of the H-box motif for DDB1 binding, we searched for a similar motif in pM27, which is known to bind DDB1, and found one (Figure 6F, upper panel). To examine its predictive value, we searched for other HCMV proteins with an H-box motif and identified pRL1 (Figures 6F, lower panel, and S4A). pRL1 precipitated DDB1 upon transfection (Figure 6G, left panel) and infection (Figure 6G, right panel). When the H-box motif in pRL1 was mutated (R159A), the interaction with DDB1 was abrogated (Figure 6G), indicating the predictive value of this motif and its relevance beyond pUL145.

To assess the importance of the DDB1 binding for STAT2 and HLTF degradation mediated by pUL145 in the viral context, we transferred one mutation (R35A), which abrogated DDB1 binding in transfection experiments (see above), into the HCMV genome. Consistent with our model, this mutant lost the capacity to precipitate DDB1 (Figure S4B) and did not degrade STAT2 and HLTF (Figure 7A).

Since pUL145 exploits DDB1 and CRLs to instruct STAT2 degradation, we assessed the biological relevance of this effect. We found that ΔUL145-HCMV is significantly more susceptible to IFNβ than AD169varL (Figure 7B). Since the inhibition of CRL activity by the drug MLN4924 restores STAT2 levels in HCMV-infected cells (Figure 5B), we analyzed if co-administration of MLN4924 can reinforce the antiviral activity of IFNβ and IFNγ. Consistent with its application to humans in clinical studies, MLN4924 did not exhibit relevant cytotoxicity (Figure 7C). We confirmed the antiviral activity of MLN4924 against HCMV and additionally observed an increased effect by the combined treatment, compared to the single treatment (Figure 7D). This finding implies that strategies that specifically target the immune evasins of viruses may be suitable to elude the viral antagonists to restore the complete efficacy of the host immune response.

Taken together, pUL145 constitutes a druggable viral DCAF that mimics the DDB1-recognizing interface of cellular DCAFs to exploit DDB1 and CRLs to impede antiviral immunity by proteasomal degradation of STAT2.

DISCUSSION

In the present study, we took advantage of largely neglected intra-strain differences occurring in the widely used and well-established HCMV strain AD169 to probe into viral IFN antagonism. Our analyses uncovered *UL145* as a key factor for

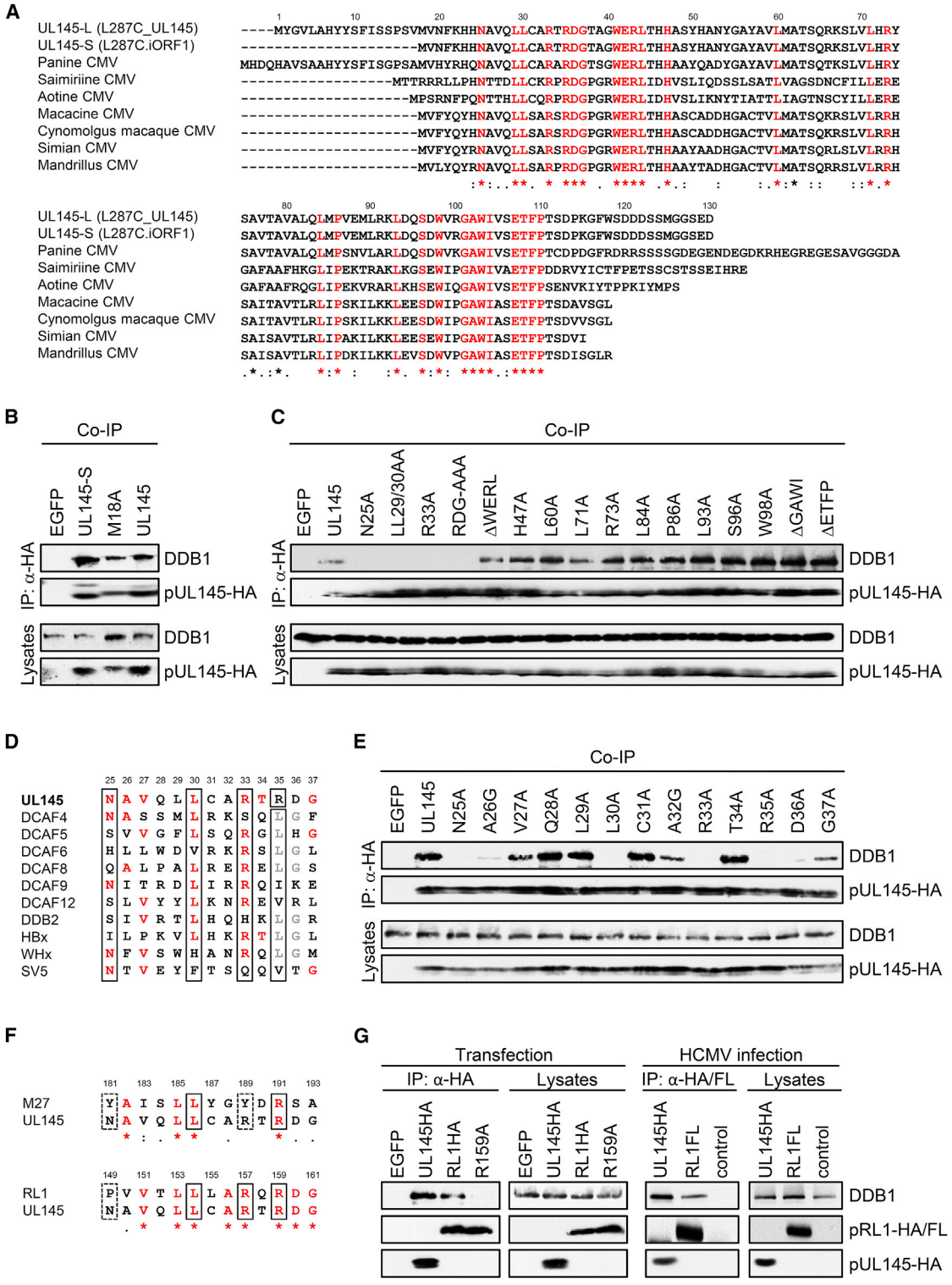

Figure 6. pUL145 Recruits DDB1 via a DCAF-like Interaction Motif

(A) The pUL145 amino acid sequence was aligned to homologous proteins encoded by primate CMVs. Conserved non-alanine residues are marked in red.

(B) 293T cells were transfected with plasmids expressing pUL145 forms. At 24 h post-transfection, lysates were generated, and an IP was performed to analyze DDB1 co-precipitation.

(C) 293T cells were transfected with plasmids expressing pUL145HA mutants. An IP was performed to analyze DDB1 co-precipitation.

(legend continued on next page)

the HCMV-encoded STAT2 degradation (Figure 3). The genomic localization of the STAT2 antagonist within the ULb′ region provides an explanation for previously observed strain-dependent differences (Le et al., 2008). The choice of the HCMV strain for use in a given experiment determines if the ULb′ region and *UL145* are present, explaining apparently contradicting results concerning STAT2 degradation (Le et al., 2008; Miller et al., 1999; Paulus et al., 2006; Weekes et al., 2014). This might also hold true for other contradictory results, which were obtained with different HCMV AD169 variants (e.g., Abate et al., 2004; Browne and Shenk, 2003). The general presence and genetic conservation of *UL145* in clinical HCMV isolates indicates that a lack of STAT2 antagonism is one result of the genomic artifacts acquired during HCMV cell culture passaging and that STAT2 degradation represents the bona fide natural phenotype of HCMV.

The generation of the AD169 BACs and their sequence determination, genome annotation, and ribosome profiling analysis provide a broad and sound basis for future studies (e.g., regarding ULb′-encoded functions). Since the relevance of several ULb′ proteins for viral pathogenesis and evasion from host immunity during establishment and maintenance of persistence or latency are well documented (e.g., Buehler et al., 2016), presumably numerous interesting, unknown mechanisms can be uncovered. In contrast to viruses—which accumulated mutations during permanent cell culture passaging, leading to alterations of the viral coding capacity and emergence of heterogeneous virus subpopulations—the AD169 BAC-cloned genomes and the mutants thereof constitute fixed sources of well-characterized HCMV variants. With the AD169varL and AD169varS BAC-derived viruses, we provide a novel experimental HCMV system without the drawback of inter-strain differences, for which we established an in-depth description of the complete coding capacities including major as well as subtle differences.

Based on ribosome profiling, we found that *UL145* actually gives rise to two discrete protein isoforms, which we termed pUL145-Long and pUL145-Short, that differ in their N termini (Figure 4). In terms of DDB1 binding and STAT2 antagonism, both isoforms were shown to be functional (Figure 5). However, their expression kinetics and abundance were strikingly different. Intriguingly, the previously known pUL145 form (corresponding to pUL145-L) was expressed only very late during infection and to a lower level (Figure 4), suggesting that pUL145-S represents the prototypic gene product encoded by the gene *UL145*. Accordingly, with the exception of human and chimpanzee CMV, all other primate CMVs encode pUL145-homologous proteins lacking the N-terminal extension (Figure 6). Recently, pUL145 has been shown to instruct the degradation of HLTF (Nightingale et al., 2018). The different pUL145 isoforms were not taken into account at that time and thus not distinguished. Because of the canonical annotation, presumably the less-abundant pUL145-L isoform was assessed. It will be interesting to determine the expression kinetics in different cell types and to test if both pUL145 isoforms similarly degrade HLTF and other targets. The loss of HLTF preceded the reduction of STAT2 (Figures S4C and S4D). We suspect HCMV can afford the delayed STAT2 degradation due to the known STAT2 inhibitory function of pp72-IE1 (Krauss et al., 2009).

Together with viruses like ZIKA, dengue, parainfluenza virus 2 (PIV2), and MCMV, HCMV represents a group of viruses that target STAT2 for proteasomal degradation (Grant et al., 2016; Le-Trilling et al., 2018; Morrison et al., 2013; Parisien et al., 2001; Trilling et al., 2011; Zimmermann et al., 2005). PIV2, MCMV, and HCMV all rely on the same cellular E3 ubiquitin ligase complex. Like HCMV, MCMV induces proteasomal degradation of STAT2 by exploiting DDB1 and CRLs to instruct ubiquitination and proteasomal degradation of STAT2. However, MCMV does not code for a pUL145 homolog and instead induces STAT2 degradation by the protein pM27. The HCMV-encoded protein pUL27, the homolog of pM27, hardly binds DDB1 and is dispensable for STAT2 degradation (Landsberg et al., 2018; Le et al., 2008). This suggests that MCMV may fail to predict functions of homologous HCMV proteins (e.g., pUL27) but discloses general principles of CMV immune evasion like STAT2 degradation and DDB1/CRL exploitation.

The existence of two functionally analogous, but genetically unrelated, HCMV- and MCMV-encoded STAT2 antagonists indicates that the capacity to induce proteasomal degradation of STAT2 by exploiting DDB1, CRLs, and the ubiquitin-proteasome system independently evolved at least two times during the evolution of betaherpesviruses. This underlines the relevance of STAT2 as an important target for CMV-mediated immune evasion. Consistent with this notion, STAT2-deficient mice exhibit an exaggerated MCMV susceptibility and succumb during the first week of MCMV infection (Le-Trilling et al., 2018).

To instruct the degradation of different host restriction factors, several viruses including HIV-1, HIV-2, HCMV, MCMV, PIV, and HBV take advantage of DDB1 and CRLs (Becker et al., 2019). This raises the interesting question of whether this is simply a coincidence or if these modular E3 ligases are particularly prone to viral exploitation. One explanation for this parallel development might be that altered CRL substrate specificities may provide some selective advantages for viruses in general (e.g., by interference with DNA-damage responses or cell-cycle regulation).

Cells regulate the CRL activity through Nedd8-conjugation (termed neddylation). Drugs such as Pevonedistat/MLN4924 inactivate the Nedd8-activating enzyme and thereby terminate CRL-mediated ubiquitination by inhibiting the neddylation of cullins. Thus, the viral exploitation of CRLs renders viruses

(D) The DDB1 interaction domain of pUL145 was aligned to the H-box motif (Li et al., 2010) of cellular DDB1-cullin-associated factors (DCAFs) and viral DDB1 interactors. The boxes mark the position of pUL145 residues found to be essential for DDB1 interaction.
(E) 293T cells were transfected with plasmids expressing UL145HA mutants. An IP with anti-HA was performed to test DDB1 co-precipitation.
(F) The H-box motif of pUL145 was used to find homologous motives in pM27 and other HCMV proteins. The search identified a highly conserved motif in the HCMV protein pRL1. See also Figure S4.
(G) To test if the presence the H-box motif in pRL1 is predictive for DDB1 interaction, pRL1 was tagged for transfection and in the virus genome. Transfected 293T as well as infected MRC-5 cells were used to perform IPs using the indicated antibodies.

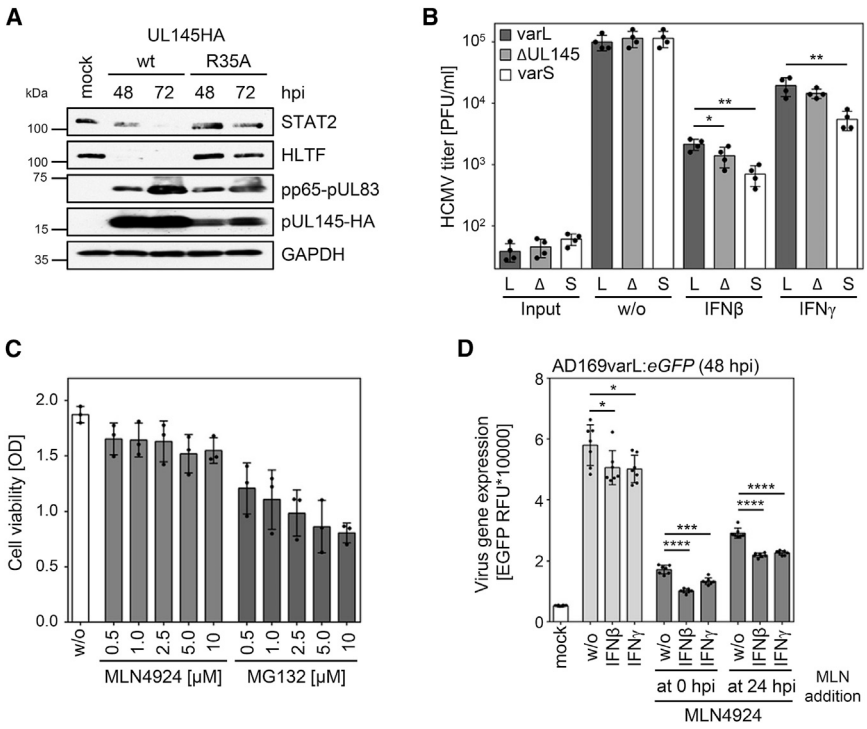

Figure 7. HCMV Exploits CRLs to Evade IFN-Mediated Antiviral Activity

(A) MRC-5 cells were infected with UL145HA virus or a virus harboring the mutation R35A in pUL145-HA. This mutation abrogates DDB1 interaction. At 72 h post-infection, lysates were generated and used for immunoblot analysis of indicated proteins. See also Figure S4.

(B) MRC-5 fibroblasts were infected (MOI 0.05) with AD169varL, AD169varS, and ΔUL145 viruses and treated with IFNβ or IFNγ (200 U/mL) at the time point of infection. For replication analysis, samples were frozen after 6 days of infection. Viral titers were determined in quadruplicate. Mean values ± SD are shown. Significance was calculated by unpaired one-tailed t test.

(C) MRC-5 cells were treated for 24 h with the indicated concentrations of MLN4924 and MG132. The toxicity was analyzed by quantification of viable cells by Orangu cell counting solution.

(D) MRC-5 cells were treated with IFNβ or IFNγ (100 U/mL) and infected with AD169varL expressing EGFP (MOI 0.3). At 0 or 24 h post-infection, cells were control treated or treated with the neddylation inhibitor MLN4924 (2 μM). At 48 h post-infection, EGFP expression was quantified by use of a microplate multireader. Bars depict mean values ± SD. Dots show the values of the individual measurements. Significance was calculated by unpaired two-tailed t test.

susceptible to compounds like MLN4924, as we have documented for HCMV and several other viruses (Le-Trilling et al., 2016). However, CRLs also regulate fundamental aspects of the cell biology (e.g., mitosis). Thus, CRL inhibitory drugs elicit strong anti-proliferative effects and are hence under investigation as potential anti-tumor drugs. As several aspects of the CRL-proteasome system are druggable (Becker et al., 2019), identification of host restriction factors, which are specifically targeted by CRLs in infected cells, may facilitate the discovery of novel drug targets and the development of more specific drugs with lesser side effects.

pUL145 represents a viral DCAF (vDCAF) that redirects the CRL activity to host proteins important for antiviral immunity (e.g., STAT2 and HLTF). The cellular DCAFs are substrate receptors of DDB1-containing ubiquitin ligases, which bind to a specific region on DDB1 and recruit substrates for ubiquitination and proteasomal degradation (Angers et al., 2006). They determine substrate recognition and are thus pivotal for regulating, for example, cell proliferation, survival, DNA repair, and genomic integrity (Lee and Zhou, 2007). Since we have identified key residues of the pUL145 DCAF-like motif, which are conserved (N25, L30, and R33) as well as specific (R35), it is tempting to speculate that an in-depth understanding of viral immune antagonists may lay the basis for the future development of drugs specifically targeting virus-exploited CRLs by discriminating between viral and cellular DCAFs.

STAR★METHODS

Detailed methods are provided in the online version of this paper and include the following:

SUPPLEMENTAL INFORMATION

Supplemental Information can be found online at https://doi.org/10.1016/j.celrep.2020.01.070.

ACKNOWLEDGMENTS

We thank Kerstin Wohlgemuth and Benjamin Katschinski for excellent technical support and our team for discussion. M.T. receives funding from the Deutsche Forschungsgemeinschaft (DFG) through RTG1949 and from the Kulturstiftung Essen. T.B. received a scholarship from the Jürgen Manchot

Stiftung. H.H. was supported by the Helmholtz Association through VISTRIE VH-VI-242. ORCIDs: V.T.K.L.-T. 0000-0002-2733-3732; M.T. 0000-0003-3659-3541.

AUTHOR CONTRIBUTIONS

V.T.K.L.-T. conceived the project, designed and performed experiments, analyzed data, prepared figures, and wrote the manuscript. T.B. designed and performed experiments, analyzed data, prepared figures, and wrote the manuscript. A.N. and N.S.-G. performed the ribosome profiling. L.S. performed experiments. S.V. did the sequence determination of BAC2 and BAC20. H.H. designed experiments. M.T. conceived the project, designed experiments, analyzed data, and wrote the manuscript. All authors reviewed and edited the manuscript.

DECLARATION OF INTERESTS

The authors declare no competing interests.

Received: May 14, 2019
Revised: November 10, 2019
Accepted: January 21, 2020
Published: February 18, 2020

REFERENCES

Abate, D.A., Watanabe, S., and Mocarski, E.S. (2004). Major human cytomegalovirus structural protein pp65 (ppUL83) prevents interferon response factor 3 activation in the interferon response. J. Virol. *78*, 10995–11006.

Angers, S., Li, T., Yi, X., MacCoss, M.J., Moon, R.T., and Zheng, N. (2006). Molecular architecture and assembly of the DDB1-CUL4A ubiquitin ligase machinery. Nature *443*, 590–593.

Atalay, R., Zimmermann, A., Wagner, M., Borst, E., Benz, C., Messerle, M., and Hengel, H. (2002). Identification and expression of human cytomegalovirus transcription units coding for two distinct Fcgamma receptor homologs. J. Virol. *76*, 8596–8608.

Becker, T., Le-Trilling, V.T.K., and Trilling, M. (2019). Cellular Cullin RING Ubiquitin Ligases: Druggable Host Dependency Factors of Cytomegaloviruses. Int. J. Mol. Sci. *20*, E1636.

Borst, E.M., Hahn, G., Koszinowski, U.H., and Messerle, M. (1999). Cloning of the human cytomegalovirus (HCMV) genome as an infectious bacterial artificial chromosome in Escherichia coli: a new approach for construction of HCMV mutants. J. Virol. *73*, 8320–8329.

Bradley, A.J., Lurain, N.S., Ghazal, P., Trivedi, U., Cunningham, C., Baluchova, K., Gatherer, D., Wilkinson, G.W., Dargan, D.J., and Davison, A.J. (2009). High-throughput sequence analysis of variants of human cytomegalovirus strains Towne and AD169. J. Gen. Virol. *90*, 2375–2380.

Browne, E.P., and Shenk, T. (2003). Human cytomegalovirus UL83-coded pp65 virion protein inhibits antiviral gene expression in infected cells. Proc. Natl. Acad. Sci. USA *100*, 11439–11444.

Buehler, J., Zeltzer, S., Reitsma, J., Petrucelli, A., Umashankar, M., Rak, M., Zagallo, P., Schroeder, J., Terhune, S., and Goodrum, F. (2016). Opposing Regulation of the EGF Receptor: A Molecular Switch Controlling Cytomegalovirus Latency and Replication. PLoS Pathog. *12*, e1005655.

Cha, T.A., Tom, E., Kemble, G.W., Duke, G.M., Mocarski, E.S., and Spaete, R.R. (1996). Human cytomegalovirus clinical isolates carry at least 19 genes not found in laboratory strains. J. Virol. *70*, 78–83.

Chee, M.S., Bankier, A.T., Beck, S., Bohni, R., Brown, C.M., Cerny, R., Horsnell, T., Hutchison, C.A., 3rd, Kouzarides, T., Martignetti, J.A., et al. (1990). Analysis of the protein-coding content of the sequence of human cytomegalovirus strain AD169. Curr. Top. Microbiol. Immunol. *154*, 125–169.

Dargan, D.J., Douglas, E., Cunningham, C., Jamieson, F., Stanton, R.J., Baluchova, K., McSharry, B.P., Tomasec, P., Emery, V.C., Percivalle, E., et al. (2010). Sequential mutations associated with adaptation of human cytomegalovirus to growth in cell culture. J. Gen. Virol. *91*, 1535–1546.

Emanuele, M.J., Elia, A.E., Xu, Q., Thoma, C.R., Izhar, L., Leng, Y., Guo, A., Chen, Y.N., Rush, J., Hsu, P.W., et al. (2011). Global identification of modular cullin-RING ligase substrates. Cell *147*, 459–474.

Gil, M.P., Bohn, E., O'Guin, A.K., Ramana, C.V., Levine, B., Stark, G.R., Virgin, H.W., and Schreiber, R.D. (2001). Biologic consequences of Stat1-independent IFN signaling. Proc. Natl. Acad. Sci. USA *98*, 6680–6685.

Grant, A., Ponia, S.S., Tripathi, S., Balasubramaniam, V., Miorin, L., Sourisseau, M., Schwarz, M.C., Sánchez-Seco, M.P., Evans, M.J., Best, S.M., and García-Sastre, A. (2016). Zika Virus Targets Human STAT2 to Inhibit Type I Interferon Signaling. Cell Host Microbe *19*, 882–890.

Hahn, G., Khan, H., Baldanti, F., Koszinowski, U.H., Revello, M.G., and Gerna, G. (2002). The human cytomegalovirus ribonucleotide reductase homolog UL45 is dispensable for growth in endothelial cells, as determined by a BAC-cloned clinical isolate of human cytomegalovirus with preserved wild-type characteristics. J. Virol. *76*, 9551–9555.

Heiden, D., Saranchuk, P., Tun, N., Audoin, B., Cohn, J., Durier, N., Holland, G., Drew, W.L., and 't Hoen, E. (2014). We urge WHO to act on cytomegalovirus retinitis. Lancet Glob. Health *2*, e76–e77.

Hengel, H., Esslinger, C., Pool, J., Goulmy, E., and Koszinowski, U.H. (1995). Cytokines restore MHC class I complex formation and control antigen presentation in human cytomegalovirus-infected cells. J. Gen. Virol. *76*, 2987–2997.

Hengel, H., Brune, W., and Koszinowski, U.H. (1998). Immune evasion by cytomegalovirus–survival strategies of a highly adapted opportunist. Trends Microbiol. *6*, 190–197.

Hirt, B. (1967). Selective extraction of polyoma DNA from infected mouse cell cultures. J. Mol. Biol. *26*, 365–369.

Krauss, S., Kaps, J., Czech, N., Paulus, C., and Nevels, M. (2009). Physical requirements and functional consequences of complex formation between the cytomegalovirus IE1 protein and human STAT2. J. Virol. *83*, 12854–12870.

Landsberg, C.D., Megger, D.A., Hotter, D., Rückborn, M.U., Eilbrecht, M., Rashidi-Alavijeh, J., Howe, S., Heinrichs, S., Sauter, D., Sitek, B., et al. (2018). A Mass Spectrometry-Based Profiling of Interactomes of Viral DDB1- and Cullin Ubiquitin Ligase-Binding Proteins Reveals NF-κB Inhibitory Activity of the HIV-2-Encoded Vpx. Front. Immunol. *9*, 2978.

Langmead, B., Trapnell, C., Pop, M., and Salzberg, S.L. (2009). Ultrafast and memory-efficient alignment of short DNA sequences to the human genome. Genome Biol. *10*, R25.

Le, V.T.K., Trilling, M., Wilborn, M., Hengel, H., and Zimmermann, A. (2008). Human cytomegalovirus interferes with signal transducer and activator of transcription (STAT) 2 protein stability and tyrosine phosphorylation. J. Gen. Virol. *89*, 2416–2426.

Le, V.T.K., Trilling, M., and Hengel, H. (2011). The cytomegaloviral protein pUL138 acts as potentiator of tumor necrosis factor (TNF) receptor 1 surface density to enhance ULb'-encoded modulation of TNF-α signaling. J. Virol. *85*, 13260–13270.

Le Roy, E., Mühlethaler-Mottet, A., Davrinche, C., Mach, B., and Davignon, J.L. (1999). Escape of human cytomegalovirus from HLA-DR-restricted CD4(+) T-cell response is mediated by repression of gamma interferon-induced class II transactivator expression. J. Virol. *73*, 6582–6589.

Le-Trilling, V.T.K., and Trilling, M. (2015). Attack, parry and riposte: molecular fencing between the innate immune system and human herpesviruses. Tissue Antigens *86*, 1–13.

Le-Trilling, V.T.K., Megger, D.A., Katschinski, B., Landsberg, C.D., Rückborn, M.U., Tao, S., Krawczyk, A., Bayer, W., Drexler, I., Tenbusch, M., et al. (2016). Broad and potent antiviral activity of the NAE inhibitor MLN4924. Sci. Rep. *6*, 19977.

Le-Trilling, V.T.K., Wohlgemuth, K., Rückborn, M.U., Jagnjic, A., Maaßen, F., Timmer, L., Katschinski, B., and Trilling, M. (2018). STAT2-Dependent Immune Responses Ensure Host Survival despite the Presence of a Potent Viral Antagonist. J. Virol. *92*, e00296–18.

Lee, J., and Zhou, P. (2007). DCAFs, the missing link of the CUL4-DDB1 ubiquitin ligase. Mol. Cell *26*, 775–780.

Lee, C.J., An, H.J., Kim, S.M., Yoo, S.M., Park, J., Lee, G.E., Kim, W.Y., Kim, D.J., Kang, H.C., Lee, J.Y., et al. (2020). FBXW7-mediated stability regulation of signal transducer and activator of transcription 2 in melanoma formation. Proc. Natl. Acad. Sci. USA *117*, 584–594.

Li, T., Robert, E.I., van Breugel, P.C., Strubin, M., and Zheng, N. (2010). A promiscuous α-helical motif anchors viral hijackers and substrate receptors to the CUL4-DDB1 ubiquitin ligase machinery. Nat. Struct. Mol. Biol. *17*, 105–111.

Ljungman, P., Brand, R., Hoek, J., de la Camara, R., Cordonnier, C., Einsele, H., Styczynski, J., Ward, K.N., and Cesaro, S.; Infectious Diseases Working Party of the European Group for Blood and Marrow Transplantation (2014). Donor cytomegalovirus status influences the outcome of allogeneic stem cell transplant: a study by the European group for blood and marrow transplantation. Clin. Infect. Dis. *59*, 473–481.

Loenen, W.A., Bruggeman, C.A., and Wiertz, E.J. (2001). Immune evasion by human cytomegalovirus: lessons in immunology and cell biology. Semin. Immunol. *13*, 41–49.

Ludwig, A., and Hengel, H. (2009). Epidemiological impact and disease burden of congenital cytomegalovirus infection in Europe. Euro Surveill. *14*, 26–32.

Megger, D.A., Philipp, J., Le-Trilling, V.T.K., Sitek, B., and Trilling, M. (2017). Deciphering of the Human Interferon-Regulated Proteome by Mass Spectrometry-Based Quantitative Analysis Reveals Extent and Dynamics of Protein Induction and Repression. Front. Immunol. *8*, 1139.

Miller, D.M., Rahill, B.M., Boss, J.M., Lairmore, M.D., Durbin, J.E., Waldman, J.W., and Sedmak, D.D. (1998). Human cytomegalovirus inhibits major histocompatibility complex class II expression by disruption of the Jak/Stat pathway. J. Exp. Med. *187*, 675–683.

Miller, D.M., Zhang, Y., Rahill, B.M., Waldman, W.J., and Sedmak, D.D. (1999). Human cytomegalovirus inhibits IFN-alpha-stimulated antiviral and immunoregulatory responses by blocking multiple levels of IFN-alpha signal transduction. J. Immunol. *162*, 6107–6113.

Morrison, J., Laurent-Rolle, M., Maestre, A.M., Rajsbaum, R., Pisanelli, G., Simon, V., Mulder, L.C., Fernandez-Sesma, A., and García-Sastre, A. (2013). Dengue virus co-opts UBR4 to degrade STAT2 and antagonize type I interferon signaling. PLoS Pathog. *9*, e1003265.

Murphy, E., Yu, D., Grimwood, J., Schmutz, J., Dickson, M., Jarvis, M.A., Hahn, G., Nelson, J.A., Myers, R.M., and Shenk, T.E. (2003). Coding potential of laboratory and clinical strains of human cytomegalovirus. Proc. Natl. Acad. Sci. USA *100*, 14976–14981.

Nightingale, K., Lin, K.M., Ravenhill, B.J., Davies, C., Nobre, L., Fielding, C.A., Ruckova, E., Fletcher-Etherington, A., Soday, L., Nichols, H., et al. (2018). High-Definition Analysis of Host Protein Stability during Human Cytomegalovirus Infection Reveals Antiviral Factors and Viral Evasion Mechanisms. Cell Host Microbe. *24*, 447–460.e411.

Notredame, C., Higgins, D.G., and Heringa, J. (2000). T-Coffee: A novel method for fast and accurate multiple sequence alignment. J. Mol. Biol. *302*, 205–217.

Parisien, J.P., Lau, J.F., Rodriguez, J.J., Sullivan, B.M., Moscona, A., Parks, G.D., Lamb, R.A., and Horvath, C.M. (2001). The V protein of human parainfluenza virus 2 antagonizes type I interferon responses by destabilizing signal transducer and activator of transcription 2. Virology *283*, 230–239.

Paulus, C., Krauss, S., and Nevels, M. (2006). A human cytomegalovirus antagonist of type I IFN-dependent signal transducer and activator of transcription signaling. Proc. Natl. Acad. Sci. USA *103*, 3840–3845.

Powers, C., DeFilippis, V., Malouli, D., and Früh, K. (2008). Cytomegalovirus immune evasion. Curr. Top. Microbiol. Immunol. *325*, 333–359.

Rafailidis, P.I., Mourtzoukou, E.G., Varbobitis, I.C., and Falagas, M.E. (2008). Severe cytomegalovirus infection in apparently immunocompetent patients: a systematic review. Virol. J. *5*, 47.

Robinson, J.T., Thorvaldsdóttir, H., Winckler, W., Guttman, M., Lander, E.S., Getz, G., and Mesirov, J.P. (2011). Integrative genomics viewer. Nat. Biotechnol. *29*, 24–26.

Sainz, B., Jr., LaMarca, H.L., Garry, R.F., and Morris, C.A. (2005). Synergistic inhibition of human cytomegalovirus replication by interferon-alpha/beta and interferon-gamma. Virol. J. *2*, 14.

Samuel, C.E. (2001). Antiviral actions of interferons. Clin. Microbiol. Rev. *14*, 778–809.

Schmidt-Hieber, M., Labopin, M., Beelen, D., Volin, L., Ehninger, G., Finke, J., Socié, G., Schwerdtfeger, R., Kröger, N., Ganser, A., et al. (2013). CMV serostatus still has an important prognostic impact in de novo acute leukemia patients after allogeneic stem cell transplantation: a report from the Acute Leukemia Working Party of EBMT. Blood *122*, 3359–3364.

Sen, G.C. (2001). Viruses and interferons. Annu. Rev. Microbiol. *55*, 255–281.

Sinzger, C., Hahn, G., Digel, M., Katona, R., Sampaio, K.L., Messerle, M., Hengel, H., Koszinowski, U., Brune, W., and Adler, B. (2008). Cloning and sequencing of a highly productive, endotheliotropic virus strain derived from human cytomegalovirus TB40/E. J. Gen. Virol. *89*, 359–368.

Soucy, T.A., Smith, P.G., Milhollen, M.A., Berger, A.J., Gavin, J.M., Adhikari, S., Brownell, J.E., Burke, K.E., Cardin, D.P., Critchley, S., et al. (2009). An inhibitor of NEDD8-activating enzyme as a new approach to treat cancer. Nature *458*, 732–736.

Stark, G.R., and Darnell, J.E., Jr. (2012). The JAK-STAT pathway at twenty. Immunity *36*, 503–514.

Stark, G.R., Kerr, I.M., Williams, B.R., Silverman, R.H., and Schreiber, R.D. (1998). How cells respond to interferons. Annu. Rev. Biochem. *67*, 227–264.

Stern-Ginossar, N., Weisburd, B., Michalski, A., Le, V.T., Hein, M.Y., Huang, S.X., Ma, M., Shen, B., Qian, S.B., Hengel, H., et al. (2012). Decoding human cytomegalovirus. Science *338*, 1088–1093.

Tischer, B.K., von Einem, J., Kaufer, B., and Osterrieder, N. (2006). Two-step red-mediated recombination for versatile high-efficiency markerless DNA manipulation in Escherichia coli. Biotechniques *40*, 191–197.

Trilling, M., Le, V.T.K., Zimmermann, A., Ludwig, H., Pfeffer, K., Sutter, G., Smith, G.L., and Hengel, H. (2009). Gamma interferon-induced interferon regulatory factor 1-dependent antiviral response inhibits vaccinia virus replication in mouse but not human fibroblasts. J. Virol. *83*, 3684–3695.

Trilling, M., Le, V.T.K., Fiedler, M., Zimmermann, A., Bleifuss, E., and Hengel, H. (2011). Identification of DNA-damage DNA-binding protein 1 as a conditional essential factor for cytomegalovirus replication in interferon-γ-stimulated cells. PLoS Pathog. *7*, e1002069.

Trilling, M., Bellora, N., Rutkowski, A.J., de Graaf, M., Dickinson, P., Robertson, K., Prazeres da Costa, O., Ghazal, P., Friedel, C.C., Albà, M.M., and Dölken, L. (2013). Deciphering the modulation of gene expression by type I and II interferons combining 4sU-tagging, translational arrest and in silico promoter analysis. Nucleic Acids Res. *41*, 8107–8125.

Venables, W.N., and Ripley, B.D. (2002). Modern Applied Statistics with S (Springer-Verlag).

Wagner, M., Gutermann, A., Podlech, J., Reddehase, M.J., and Koszinowski, U.H. (2002). Major histocompatibility complex class I allele-specific cooperative and competitive interactions between immune evasion proteins of cytomegalovirus. J. Exp. Med. *196*, 805–816.

Weekes, M.P., Tomasec, P., Huttlin, E.L., Fielding, C.A., Nusinow, D., Stanton, R.J., Wang, E.C., Aicheler, R., Murrell, I., Wilkinson, G.W., et al. (2014). Quantitative temporal viromics: an approach to investigate host-pathogen interaction. Cell *157*, 1460–1472.

Zimmermann, A., Trilling, M., Wagner, M., Wilborn, M., Bubic, I., Jonjic, S., Koszinowski, U., and Hengel, H. (2005). A cytomegaloviral protein reveals a dual role for STAT2 in IFN-gamma signaling and antiviral responses. J. Exp. Med. *201*, 1543–1553.

STAR★METHODS

KEY RESOURCES TABLE

REAGENT or RESOURCE	SOURCE	IDENTIFIER
Antibodies		
Rabbit polyclonal anti-GAPDH	Santa Cruz Biotechnology	Cat# sc-25778; RRID:AB_10167668
Mouse monoclonal anti-HA (clone HA-7)	Sigma-Aldrich	Cat# H3663; RRID:AB_262051
Rabbit polyclonal anti-HA	Sigma-Aldrich	Cat# H6908; RRID:AB_260070
Mouse monoclonal anti-FLAG (clone M2)	Sigma-Aldrich	Cat# F3165; RRID:AB_259529
Mouse monoclonal anti-JAK1	BD Biosciences	Cat# 610232; RRID:AB_397627
Rabbit monoclonal anti-JAK2	Cell Signaling Technology	Cat# 3230; RRID:AB_2128522
Rabbit polyclonal anti-STAT1	Santa Cruz Biotechnology	Cat# sc-346; RRID:AB_632435
Rabbit polyclonal anti-STAT2	Santa Cruz Biotechnology	Cat# sc-476; RRID:AB_632437
Mouse monoclonal anti-IRF9	Santa Cruz Biotechnology	Cat# sc-365893; RRID:AB_10846858
Rabbit polyclonal anti-DDB1	Bethyl Laboratories	Cat# A300-462A
Rabbit monoclonal anti-HLTF	Abcam	Cat# ab183042
Mouse monoclonal anti-HCMV-pp65 (clone 3A12)	Abcam	Cat# ab6503; RRID:AB_305525
Mouse monoclonal anti-HCMV-pp72 (clone L-14)	Stipan Jonjic (Rijeka, Croatia)	N/A
Mouse monoclonal anti-HCMV-gB (clone 27-156)	Stipan Jonjic (Rijeka, Croatia)	N/A
Mouse monoclonal anti-Cytomegalovirus (clones DDG9 and CCH2)	Agilent	Cat# M0854
Mouse monoclonal anti-MCMV-pp89 (CROMA101)	Stipan Jonjic (Rijeka, Croatia)	N/A
Bacterial and Virus Strains		
E. coli GS1783	Tischer et al., 2006	N/A
E. coli DH10B	Thermo Fisher	N/A
E. coli XL1-Blue F	Stratagene	N/A
HCMV AD169varL	Le et al., 2011	N/A
HCMV AD169varS	Le et al., 2011	N/A
HCMV TB40	Sinzger et al., 2008	N/A
HCMV AD169-BAC2	Le et al., 2011	N/A
HCMV AD169-BAC20	This Paper	N/A
HCMV AD169-BAC2Δgpt:EGFP	Le-Trilling et al., 2016	N/A
HCMV AD169-BAC20Δgpt:EGFP	Le-Trilling et al., 2016	N/A
HCMV AD169-BAC2ΔUL148-150	This paper	N/A
HCMV AD169-BAC2ΔUL148-133	This paper	N/A
HCMV AD169-BAC2ΔUL148A-150	This paper	N/A
HCMV AD169-BAC2ΔUL148-146	This paper	N/A
HCMV AD169-BAC2ΔUL139-133	This paper	N/A
HCMV AD169-BAC2ΔUL145	This paper	N/A
HCMV TB40-BAC4ΔUL145	This paper	N/A
HCMV AD169-BAC2ΔUL145:UL145HA	This paper	N/A
HCMV AD169-BAC20Δgpt:UL145HA	This paper	N/A
HCMV AD169-BAC2-UL145HA	This paper	N/A
HCMV AD169-BAC2-UL145HA:ATG1mut	This paper	N/A
HCMV AD169-BAC2-UL145HA:ATG2mut	This paper	N/A

(*Continued on next page*)

Continued

REAGENT or RESOURCE	SOURCE	IDENTIFIER
HCMV AD169-BAC2-UL145HA:R35A	This paper	N/A
HCMV AD169-BAC2-RL1FLAG	This paper	N/A
Chemicals, Peptides, and Recombinant Proteins		
Recombinant human IFN-α2	PBL Assay Science	Cat# 11101
Recombinant human IFN-β	PeproTech	Cat# 300-02BC
Recombinant human IFN-γ	PBL Assay Science	Cat# 11500
MG132	Sigma-Aldrich	Cat# C2211
MLN4924	Active Biochem	Cat# A-1139
Ganciclovir	Sigma-Aldrich	Cat# G2536
Critical Commercial Assays		
QuikChange II XL Site Directed Mutagenesis Kit	Agilent	Cat# 200522
Orangu Cell Counting Solution	Cell Guidance Systems	Cat# OR01-3000
Deposited Data		
AD169-BAC2 genome sequence	GenBank	GenBank: MN900952
AD169-BAC20 genome sequence	GenBank	GenBank: MN920393
Experimental Models: Cell Lines		
human MRC-5	ATCC	CCL-171
human HeLa	ATCC	CCL-2
human HEK293T	ATCC	CRL-11268
Oligonucleotides		
See Tables S4 and S5 for oligonucleotides used for the construction of recombinant HCMV mutants and site-directed mutagenesis, respectively.	This paper	N/A
Recombinant DNA		
pISRE-Luc	Stratagene	N/A
PMZ3F-STAT2-SPA	Landsberg et al., 2018	N/A
pIRES2-EGFP-M27HA	Trilling et al., 2011	N/A
pIRES2-EGFP-UL145HA	Le et al., 2011	N/A
pcDNA3.1-Intron-UL145HA	Le et al., 2011	N/A
pcDNA3.1-Intron-UL145HA-M18A	This paper	N/A
pcDNA3.1-Intron-UL145HA-N25A	This paper	N/A
pcDNA3.1-Intron-UL145HA-LL29/30AA	This paper	N/A
pcDNA3.1-Intron-UL145HA-R33A	This paper	N/A
pcDNA3.1-Intron-UL145HA-RDG35/36/37AAA	This paper	N/A
pcDNA3.1-Intron-UL145HA-ΔWERL	This paper	N/A
pcDNA3.1-Intron-UL145HA-H47A	This paper	N/A
pcDNA3.1-Intron-UL145HA-L60A	This paper	N/A
pcDNA3.1-Intron-UL145HA-L71A	This paper	N/A
pcDNA3.1-Intron-UL145HA-R73A	This paper	N/A
pcDNA3.1-Intron-UL145HA-L84A	This paper	N/A
pcDNA3.1-Intron-UL145HA-P86A	This paper	N/A
pcDNA3.1-Intron-UL145HA-L93A	This paper	N/A
pcDNA3.1-Intron-UL145HA-S96A	This paper	N/A
pcDNA3.1-Intron-UL145HA-W98A	This paper	N/A
pcDNA3.1-Intron-UL145HA-ΔGAWI	This paper	N/A
pcDNA3.1-Intron-UL145HA-ΔETFP	This paper	N/A

(*Continued on next page*)

Continued

REAGENT or RESOURCE	SOURCE	IDENTIFIER
pcDNA3.1-Intron-UL145HA-A26G	This paper	N/A
pcDNA3.1-Intron-UL145HA-V27A	This paper	N/A
pcDNA3.1-Intron-UL145HA-Q28A	This paper	N/A
pcDNA3.1-Intron-UL145HA-L29A	This paper	N/A
pcDNA3.1-Intron-UL145HA-L30A	This paper	N/A
pcDNA3.1-Intron-UL145HA-C31A	This paper	N/A
pcDNA3.1-Intron-UL145HA-A32G	This paper	N/A
pcDNA3.1-Intron-UL145HA-T34A	This paper	N/A
pcDNA3.1-Intron-UL145HA-R35A	This paper	N/A
pcDNA3.1-Intron-UL145HA-D36A	This paper	N/A
pcDNA3.1-Intron-UL145HA-G37A	This paper	N/A
pIRES2-EGFP-RL1HA	This paper	N/A
pIRES2-EGFP-RL1HA-R159A	This paper	N/A
Software and Algorithms		
Newbler 2.6	454 Life Sciences	N/A
Geneious	Biomatters, Inc.	https://www.geneious.com
MicroWin (Mithras2 LB 943)	Berthold Technologies	N/A
T-Coffee	Notredame et al., 2000	https://www.ebi.ac.uk/Tools/msa/tcoffee/
GraphPad Prism	GraphPad Software Inc.	https://www.graphpad.com
Bowtie 1.1.2	Langmead et al., 2009	http://bowtie-bio.sourceforge.net/manual.shtml
R 3.5.0	Venables and Ripley, 2002	https://www.r-project.org/
IGV 2.4.2	Robinson et al., 2011	https://software.broadinstitute.org/software/igv/home

LEAD CONTACT AND MATERIALS AVAILABILITY

Further information and requests for resources and reagents should be directed to and will be fulfilled by the Lead Contact, Mirko Trilling (Mirko.Trilling@uk-essen.de). All unique/stable reagents generated in this study are available from the Lead Contact without restriction.

EXPERIMENTAL MODEL AND SUBJECT DETAILS

Cells, viruses, and infection

Human MRC-5 fibroblasts (ATCC CCL-171, passages 10-18, male), HeLa (ATCC CCL-2, female) and HEK293T (ATCC CRL-11268, female) cells were grown in Dulbecco's minimal essential medium (DMEM) supplemented with 10% fetal calf serum (FCS), penicillin, streptomycin, and 2 mM glutamine at 37°C in 5% CO_2. MRC-5 fibroblasts were only used in defined passages (10-18), limiting the risk of contamination due to extensive passaging over long time periods. In addition, the HCMV AD169 strain used for the experiments is only permissive in human fibroblasts, further limiting the chances that the MRC-5 cells have been contaminated with another cell type. HeLa and HEK293T cells were regularly monitored for morphology and maintenance of the typically high transfection efficiency.

The HCMV strain AD169varL (Le et al., 2011) and the endotheliotropic strain TB40/E (Sinzger et al., 2008) reconstituted from the respective BAC clones AD169-BAC2 and TB40-BAC4, respectively, were described in Le et al. (2011) and Sinzger et al. (2008). Virus stocks were prepared as described previously by propagating HCMV in MRC-5 fibroblasts (Hengel et al., 1995). HCMV infection was enhanced by centrifugation at 800 g for 30 min.

METHOD DETAILS

Generation of AD169 bacterial artificial chromosomes

For the cloning of the AD169-HCMV genome as bacterial artificial chromosomes (BACs) in *E. coli*, we followed described procedures (Hahn et al., 2002). Briefly, MRC-5 fibroblasts were transfected with the plasmid pEB1097 (Borst et al., 1999) containing a tk-gpt-bac-cassette flanked with HCMV homologous sequences of US1-US2 (AD169 nt 192648 - 193360; GenBank accession number X17403)

on the right side and US6-US7 (AD169 nt 195705 - 197398) on the left side of the cassette. At 24 h post transfection, cells were infected with AD169varL (MOI 5). Recombinant viruses were enriched by three rounds of selection with 25 μM xanthine and 100 μM mycophenoloic acid. Circular viral genomes were extracted by Hirt extraction (Hirt, 1967) and electroporated into DH10B *E. coli*. BAC-containing bacteria were selected on agar plates containing 12.5 μg/ml chloramphenicol. BAC DNA was prepared from colonies for control restriction digest. The BAC-cloned AD169 genomes of AD169-BAC2 and AD169-BAC20 were used for further analysis.

Sequence determination of AD169-BAC2 and AD169-BAC20 genomes

DNA of AD169-BAC2 and AD169-BAC20, which genetically correspond to AD169varL and AD169varS, respectively, was isolated using a midiprep purification kit (Macherey-Nagel) and subjected to next generation sequencing. The DNA was sheared with Covaris S2. Libraries were generated utilizing the rapid library kit and sequenced with Titanium chemistry on a 454 FLX instrument (Roche). Reads with 1616-fold and 2109-fold coverage for AD169-BAC2 and AD169-BAC20, respectively, were mapped to our scaffold sequence data using Newbler 2.6 software. Results of a *de novo* assembly using Newbler 2.6 confirmed the results of the mapping. Alignments were performed with Geneious.

The sequences were annotated according to the ORFs listed in Tables S4, S5, and S7 published in Stern-Ginossar et al. (2012). The annotated sequences were deposited (GenBank: MN900952 and MN920393).

Ribosome profiling, sequence alignments, normalization, and clustering

For the preparation of the ribosome profiling samples, AD169-BAC2 and AD69-BAC20 infected cells were pretreated with cycloheximide (100 μg/ml) for 1 minute. The cells were lysed in lysis buffer (20 mM Tris 7.5, 150 mM NaCl, 5 mM $MgCl_2$, 1 mM dithiothreitol, 8% glycerol) supplemented with 0.5% triton, 30 U/ml Turbo DNase (Ambion) and 100 μg/ml cycloheximide. Lysates were subjected to ribosome footprinting by nuclease treatment. Footprint fragments were purified by denaturating PAGE, and deep sequencing libraries were generated from these fragments as previously described (Stern-Ginossar et al., 2012). These libraries were analyzed by sequencing on the Illumina HiSeq.

Prior to the sequence alignment, linker and polyA sequences were removed from the 3′ ends of reads. Bowtie v0.12.7 (5) (allowing up to 2 mismatches) was used to perform the alignments. First, reads that aligned to human rRNA sequences were discarded. All remaining reads were aligned to the concatenated HCMV genome (NC_006273.2 and FJ527563.1). Finally, still-unaligned reads were aligned to 200 bp sequences that spanned splice junctions. Reads with unique alignments were used to compute the total number of reads at each position. Footprint densities were calculated in units of reads per kilobase per million (RPKM) in order to normalize for gene length and total reads per sequencing run.

Generation of recombinant HCMV mutants and cloning of expression plasmids

Recombinant HCMV mutants were generated according to previously published procedures (Tischer et al., 2006; Wagner et al., 2002) using AD169-BAC2, AD169-BAC20, and TB40-BAC4. For the construction of the HCMV deletion mutants, a PCR fragment was generated (see Table S4 for primer sequences) using the plasmid pSLFRTKn (Atalay et al., 2002) as template DNA. The PCR fragments containing a kanamycin resistance gene were inserted into the parental BAC by homologous recombination in *E. coli*. The inserted cassette replaces the target sequence which was defined by flanking sequences in the primers. This cassette is flanked by frt-sites which can be used to remove the kanamycin resistance gene by flp-mediated recombination. The removal of the cassette results in a single remaining frt-site.

The construction of EGFP-expressing HCMVs was described in Le-Trilling et al. (2016). Briefly, the AD169varL:EGFP HCMV was generated based on the pAD169-BAC2 (Le et al., 2008). An frt-site-flanked fragment encompassing the EGFP gene controlled by the MCMV MIEP was introduced into AD169varLΔgpt (harboring an frt-site instead of the *gpt* gene of the BAC cassette) by flp-mediated recombination. For the generation of the AD169-BAC20 virus expressing pUL145-HA (AD169varS:UL145-HA), an frt-site-flanked fragment encompassing the human EF1 promoter in front of the *UL145-HA* gene was introduced into AD169-BAC20Δgpt (which harbored an frt-site instead of the *gpt* gene in the BAC cassette) by flp-mediated recombination. AD169-BAC2-ΔUL145:UL145HA was constructed by the same procedure using AD169-BAC2ΔUL145 as parental BAC.

The virus expressing UL145-HA under the control of the endogenous viral promoter was generated by two-step red-mediated recombination (Tischer et al., 2006) using the primers AD169-UL145HA-Kana1 and AD169-UL145HA-Kana2 (see Table S4) for PCR amplification and AD169-BAC2 as parental BAC. ATG1 and ATG2 of UL145 were mutated by use of the primers AD169-UL145-ATG1mut-Kana1/2 and AD169-UL145-ATG2mut-Kana1/2, respectively (see Table S4) with AD169-UL145HA as parental BAC. For the R35A mutant, AD169-UL145-R35A-Kana1/2 were used.

Correct mutagenesis of recombinant HCMV BACs was confirmed by southernblot and PCR analysis (data not shown). AD169-UL145HA, AD169-UL145HA:ATG1mut and AD169-UL145HA:ATG2mut, AD169-UL145HA:R35A and AD169-RL1FLAG were controlled by sequencing after PCR amplification of the respective genome region (data not shown). Recombinant HCMVs were reconstituted from HCMV BAC DNA by Superfect (QIAGEN) transfection into permissive MRC-5 cells.

The UL145 and M27 expression plasmids were described previously (Le et al., 2011; Trilling et al., 2011). Site-directed mutations were introduced using the primers listed in Table S5 and the QuikChangeII kit (Agilent) according to manufacturer's instructions. All contructs were confirmed by sequence determination of the respective coding sequence. The pISRE-Luc reporter construct was purchased from Stratagene.

Cytokines, inhibitors, transfection, and luciferase assay

Human IFN-α2 and human IFN-γ were purchased from PBL, human IFN-β from Peprotech. For the inhibition of the proteasome, MG132 (Sigma) was used. The neddylation inhibitor MLN4924 was purchased from Active Biochem and ganciclovir from Sigma.

HeLa and 293T cells were transfected by the use of polyethylenime hydrochloride reagent (PEI, Sigma) at a concentration of 3μg PEI per μg plasmid DNA.

Luciferase activity was measured according to the manufacturer's instructions (pjk) using a microplate multireader (Mithras2 LB 943; Berthold Technologies).

Immunoblot analysis

Immunoblotting was performed according to standard procedures. Briefly, cells were lysed as described (Trilling et al., 2009) and equal amounts of protein were subjected to SDS-PAGE and transferred to nitrocellulose membranes. Immunoblot analysis was performed using the following antibodies: anti-GAPDH (Santa Cruz), anti-HA (H3663 and H6908, Sigma), anti-FLAG M2 (Sigma), anti-JAK1 (BD), anti-JAK2 (Cell Signaling), anti-STAT1 (Santa Cruz), anti-STAT2 (Santa Cruz), anti-IRF9 (Santa Cruz), anti-DDB1 (Bethyl), anti-HCMV-pUL83/pp65 (Abcam), mAb anti-HCMV-pIE1/pp72 (L-14), mAb anti-HCMV-pUL55/gB (27-156), and mAb anti-MCMV-pIE1/pp89 (CROMA101). Proteins were visualized using peroxidase-coupled secondary antibodies (Dianova) and the ECL chemiluminescence system (Cell Signaling).

Immunoprecipitation (IP)

Transfected or infected cells were washed with ice cold PBS and subsequently lysed as described (Le et al., 2011; Trilling et al., 2011) by incubation for 1h on ice in the following buffer: 0.1 mM EDTA, 150 mM NaCl, 10 mM KCl, 10 mM MgCl2, 10% (v/v) glycerol, 20 mM HEPES (pH 7.4), 0.5% (v/v) NP-40, 0.1 mM PMSF, 1 mM DTT, 10 μM pepstatin A, 5 μM leupeptin, 0.1 mM Na-vanadate, Complete protease inhibitor (Roche). Lysates were cleared by centrifugation for 30 min at 4°C and 16,000 g. The IP antibody was added to the supernatant and incubated over night at 4°C in a rotating device. Immune complexes were precipitated with Protein-G-Sepharose (GE Healthcare) for 1 h at 4°C in a rotating device and washed with 150, 250, and 400 mM NaCl-containing lysis buffer. Samples were separated by SDS-PAGE for immunoblot analysis.

in-cell-ELISA (icELISA)

For the quantification of viral protein amounts in infected cells, an icELISA was applied. For the analysis, cells were fixed with 4% (w/v) paraformaldehyde/PBS, permeabelized with 1% (v/v) Triton X-100/PBS, blocked with 3% (v/v) FCS/PBS and stained with anti-HA (Sigma H3663). The ELISA reaction was started by the use of peroxidase-labeled secondary antibodies and TMB substrate. The reaction was stopped with 0.5 M HCl before the absorbance was determined using a microplate multireader (Mithras2 LB 943; Berthold Technologies).

Northernblot analysis of specific transcripts

Total RNA was extracted from cells using the RNeasy Mini Kit (QIAGEN). Total RNA was subjected to MOPS gel electrophoresis and transferred to nylon membranes using the TurboBlotter (Schleicher and Schuell). Probes were prepared by PCR with gene specific primers and digoxigenin-labeled dUTP (Roche) for detection of indicated transcripts. Hybridization and detection were performed as described by Roche manuals.

QUANTIFICATION AND STATISTICAL ANALYSIS

Quantification of fluorescence, luminescence, and optical density was performed by use of the microplate multireader Mithras2 LB 943 and MicroWin software (Berthold Technologies). The resulting data were analyzed using GraphPad Prism software. The values are reported as Mean ± standard deviation (SD) as described in the figure legends. Statistical significance was determined using Student's t test. A p value of < 0.05 was considered statistically significant.

DATA AND CODE AVAILABILITY

The AD169-BAC2 and AD169-BAC20 sequences obtained during this study were deposited at GenBank (accession numbers GenBank: MN900952 and GenBank: MN920393). Source data for Figure 2 in the paper is available in Table S2.